Høgskolen i Gjøviks rapportserie, 2007 nr. 4

Proceedings from Gjøvik Color Imaging Symposium 2007

J. Y. Hardeberg, P. Nussbaum, and I. Farup (editors)

Institutt for Informatikk og Medieteknikk

Gjøvik 2007
ISSN 0806-3176

Contents

Preface 5

Keynote Lectures 7

Rizzi & McCann: Spatial Color Vision 9

Enokson: Studies on Image Control for Better Reproduction in Offset 11

Tsumura: Appearance reproduction 12

Invited Lectures 19

Seim & Valberg: The response of primate cone-opponent cells 21

Green: Recent developments in ICC colour management 22

Parraman: Inkjet in question: adapting current colour and ink technology 24

Köppen & Franke: A Generalized Approach of Color Morphology 29

Submitted Papers 31

Bingham et al.: Digital camera RAW profiling 33

Sole & Green: Measurement of colour on translucent material viewed by reflection 40

Kirkenær: Certifying Monitor Proofing Systems 45

Thomas et al.: Additivity Based LC Display Color Characterization 50

Koirala et al.: Color Mixing and Color Separation of Pigments with Concentration Prediction 56

Makino et al.: Video-based analysis for facial skin appearance with automatic face tracking 63

Mansouri et al.: New decomposition basis for reflectance recovery 75

Gerhardt & Hardeberg: Spectral Color Reproduction versus Color Reproduction 83

Preface

For the fourth time Gjøvik University College and The Norwegian Color Research Laboratory organises an international symposium on colour imaging. Gjøvik Color Imaging Symposium 2007 takes place June 14&15, 2007, at Gjøvik University College in Gjøvik, Norway.

In these proceedings you will find short abstracts of the invited and keynote presentations, as well as extended abstract for the submitted contributions. For more information about the conference, please refer to http://www.colorlab.no/.

Gjøvik, June 2007

Prof. Jon Y. Hardeberg, Conference Chair

Keynote Lectures

Spatial Color Vision

A. Rizzi
Dip. di Tecnologie dell'Informazione, Università degli Studi di Milano, rizzi@dti.unimi.it

J. J. McCann
McCann Imaging, mccanns@tiac.net

Human vision has remarkable image processing power. It captures information over a very wide dynamic range of light intensities and spectral distributions. Unlike films and electronic sensors, visual appearances are nearly constant, despite widely variable input stimuli. Computer algorithms mimic vision by responding to the image content, as well as to the radiometric properties of individual pixels. The spatial analysis of images is the basis of appearance constancy, with both changes in spectral content and the level of light.

Today, there is a growing family of algorithms that treat/modify/enhance color information in its visual context, also known as *Spatial Color* methods (e.g. Retinex [1], ACE [2], or RSR [3]). These models are responsive to image content as well as to pixel statistics. They produce results that, due to a changing spatial configuration, can have a non-unique relationship with the physical input. For this reason, they cannot be described using convolution filters and since their behavior changes according to the image content, their impulsive response is not fixed.

They all share the idea of recomputing color of each pixel through the spatial distribution of values in the image, but a lot of differences arise according to their purpose. From this point of view, *Spatial Color Algorithms* (SCA) can be led by mainly three different goals:

- Accurately model the human vision system (HVS) predicting color appearance, [SCA-HVS Model]
- Aim to enhance images in the direction of human visual appearance, [SCA-Rendering]
- Attempt to calculate the actual reflectance of an object from the radiance (reflectance $\times$ illumination). [SCA-Reflectance]

Since SCAs can have three distinct goals, three different kind of outcomes are expected, and three different measures of performance are required.

Judging these models' performance is a challenging task and is still an open problem. Two main variables affect the final result of these algorithms: their parameters and the visual characteristics of the image they process. The term visual characteristics refers not only to the image's digital pixel values, (e.g. calibration of pixel value, the measured dynamic range of the scene, the measured dynamic range of the digital image), but also to the spatial distribution of these digital pixel values in the image. This paper discusses the visual configurations in which a Spatial Color methods show interesting, or critical behavior. We survey the more significant Spatial Color configurations including color constancy and contrast. The discussion presents the strengths and weaknesses of different algorithms, hopefully allowing a deeper understanding of their behavior and stimulating discussions about the search for a common judging ground.

References

[1] J. J. McCann, "Black Capturing a black cat in shade: past and present of Retinex color appearance models", Journal of Electronic Imaging, **13**, 36-47, 2004.

[2] A. Rizzi, C. Gatta, D. Marini, "A New Algorithm for Unsupervised Global and Local Color Correction", Pattern Recognition Letters, **24** (11), pp. 1663-1677, July 2003.

[3] E. Provenzi, M. Fierro, A. Rizzi, L. De Carli, D. Gadia, D. Marini, "Random Spray Retinex: a new Retinex implementation to investigate the local properties of the model" IEEE Transactions on Image Processing, Vol. **16**, Issue 1, pp. 162-171, January 2007.

Biography

Alessandro Rizzi took the degree in Computer Science at University of Milano and received a PhD in Information Engineering at University of Brescia (Italy). He taught Information Systems and Computer Graphics at University of Brescia and at Politecnico di Milano. Now he is assistant professor, teaching Multimedia and Human-Computer Interaction, and senior research fellow at the Department of Information Technologies at University of Milano. Since 1990 he is researching in the field of digital imaging and vision. His main research topic is the use of color information in digital images with particular attention to color perception mechanisms. He is the coordinator of the Italian Color Group.

Studies on Image Control for Better Reproduction in Offset

Emmi Enoksson
The Royal Institute of Technology, KTH, Sweden

This research work has focused on studies of image control for better reproduction in offset and has been applied practically. This research work has resulted in a survey of color management knowledge, a communication list concerning ICC profiles, an educational kit, a proposal for a new terminology and a patent concerning image adaptation. The work is divided into following three areas:

1) image classification A better understanding of image processing can avoid misunderstandings in the print and leading to more satisfied customers. To achieve optimal print quality for different images, it is important to adapt the prepress settings to the image category. Images can be divided into different categories depending on their image content, key information and tone distribution. Trials have been carried out in which the IT.8 test chart has been adapted to different image categories. The results of the image adaptation suggest that an adjustment only to low-key images (dark images) is sufficient, as even normal-key images then show a better similarity to the original image. The low-key image showed more details in dark areas.

2) color separation Two studies have been carried out. The purpose has been to investigate the knowledge level in color separation, the use of ICC-profiles and the understanding of color management in various printing houses in Sweden. This was done to identify and suggest new applications and suggested actions. These studies indicate that there is a serious problem in the graphic arts industry. The problem is that there is both an insufficient knowledge of color management and a lack of communication. There is a lack of competence and a lack of literature and instructions which can help printers to better understand the technology, and communication suffers through a lack of a common language.

3) suggested actions and the development of tools Terminology simplification is crucial for the users. A new term for separation "Compensation by Black", CB, has been suggested. A single term should make it easier for the users to understand and use the different settings which impact the image reproduction. A new tool/kit for the evaluation of ICC-profiles has been created. The goal of this educational kit is to facilitate and exemplify the practical understanding of profiles and their use for the users.

Biography

Emmi Enoksson works at the University of Dalarna in Sweden as the Head of the Graphic Arts Department, which is part of the Faculty of Engineering, with 100 students. The research she is currently conducting is part of her doctorate in image classification and optimized image reproduction at the Media Technology and Graphic Arts, Royal Institute of Technology (KTH), Stockholm, Sweden. Projects Emmi is involved in: redesigning and improving the image classification and optimized image reproduction process, examining the process from scanner to printer, and also development of pedagogic tools for evaluation of ICC-profiles. Emmi Enoksson has worked both as a lecturer in image, printing, layout and graphic software at various educational institutions, and also as an image printing consultant for printing companies and paper mills.

Appearance reproduction for 3D soft proofing, skin colour reproduction and e-commerce

Norimichi Tsumura
Graduate School of Integration Science & Department of Information and Image Sciences,
Chiba University, Japan

1. Introduction

In the process of product development, an appearance of the product is usually evaluated by directly observing the trial pieces. The shape of products can be evaluated by making the mock up or showing the computer graphics image. However, it is difficult to evaluate the appearance without making a trial piece, since they are dependent on the viewing devices, environmental illuminant. It is said that the evaluation of appearance become bottle neck in the cycle of the development. Therefore, it is required to predict the appearances for product in various industries. In this review, we will introduce our practical approaches for appearance reproduction [1] in 3D soft proofing, skin colour reproduction and e-commerce.

2. Appearance reproduction for 3D colour proof system [2]

There are many kinds of 3D prints such as beverage cans, PET bottles, snack packages, and so on in our life. In the field of B to B e-commerce system on designing and marketing of products, it is required to display the measured or simulated images of the 3D prints. Figure 1 show the software to evaluate appearance of the beverage cans. This system made by DIC Corporation in the collaboration with our laboratory. However, these images tend to be higher dynamic range than the luminance range of usual monitor, because the 3D prints are made of smooth materials such as papers, plastics, and metals that have sharp and strong specular reflection. Therefore, the images of 3D prints cannot be displayed without certain image processing for dynamic range compression.

Accurate reproduction of contrast gloss and that of color and shading are trade-off in tone mapping. For the accurate reproduction of contrast gloss, it is required to decrease luminance in non-highlight area. The resultant tone mapped images tend to be unsatisfactorily dark except highlight area. On the contrary, it is required to clip luminance in highlight area into the

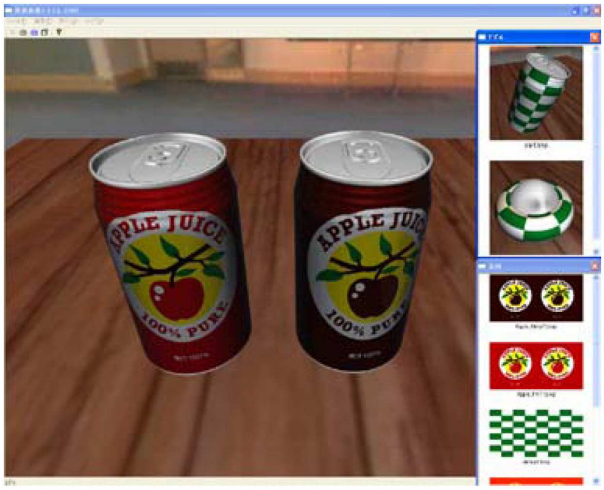

Figure 1: Software to evaluate appearance of the products (with DIC Corporation).

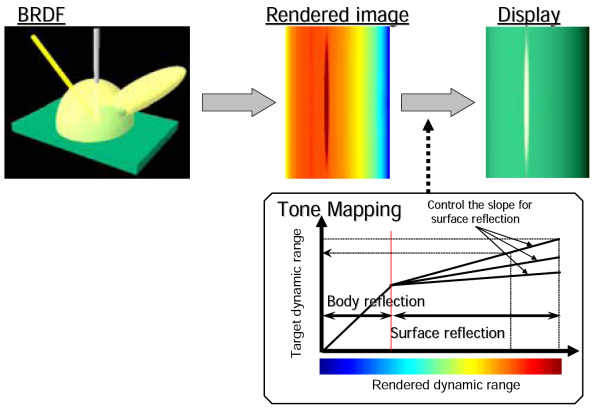

Figure 2: Rendering high dynamic range image and proposed tone mapping.

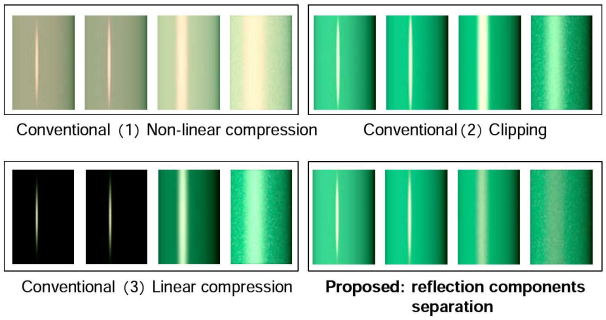

Figure 3: Resultant image by conventional and proposed range compression methods.

maximum monitor luminance for the accurate reproduction of color and shading. The resultant tone mapped images tend to have less contrast gloss than real objects.

As is shown in Figure 2, we proposed to map luminance of diffuse reflection and specular reflection in different ways. In Figure 2, the luminance on the virtual CCD on the camera is calculated in the computer by using the computer graphics techniques. The rendered luminance image is shown by pseudocolor scale in the luminance range of usual monitor. In the proposed tone mapping [2], the luminance images for diffuse and specular reflection are separately calculated. It is easy to separate diffuse and specular reflections in rendered Figure 6, since the rendered image can not be displayed in the conventional imaging system. This is because that the rendered image is expected to be high dynamic range, and the luminance image has higher dynamic range than luminance images, since the BRDF used in the rendering process is formulated as a sum of both reflections. Rendering using BRDF formula of diffuse (specular) reflection gives images of diffuse (specular) reflection. In the proposed tone mapping, only the specular reflection is mapped to the target dynamic range by controlling the slope of specular reflection component as is shown in Figure 2.

Figure 3 shows the effectiveness of the proposed method. The conventional results for (1)non-linear compression (3) linear compression show that color of diffuse components can not be reproduced in these method. The conventional results for (2) clipping show the accurate color reproduction of diffuse components, however, the relative magnitude of glossiness is not preserved compared to the real object. The result of proposed method shows the accurate color reproduction of diffuse components and preservation of the relative magnitude of glossiness.

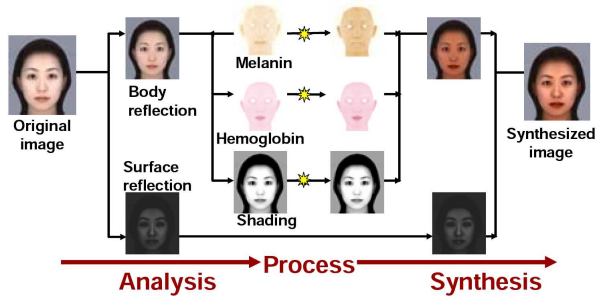

Figure 4: Image based skin color analysis and synthesis (with Kao Corporation).

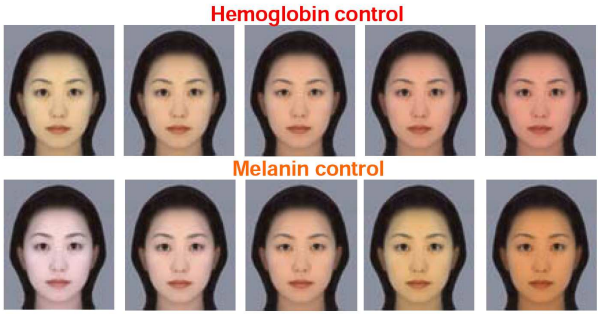

Figure 5: Skin color synthesis with the change of pigmentation.

3. Appearance reproduction for skin colour reproduction [3]

The reproduction of human skin color may be considered as the most important function of various imaging systems. With the recent progress of various imaging systems, such as mobile phones with CCD cameras, cosmetic advisory systems, and telemedicine systems, the reproduction of skin color has become increasingly important for image communication, cosmetic recommendations, medical diagnosis, and so on. We proposed an E-cosmetic function for digital images, based on physics and physiologically-based image processing. In this method, the scattering in the skin is modelled in a simple linear form in the optical density domain, and inverse optical scattering is performed by a simple inverse matrix operation. Figure 4 shows the schematic of flow in the proposed image-based skin color and texture analysis/synthesis. The original image is separated into the images of surface and body reflection based on polarized illumination, and the body reflection image is analyzed by independent component analysis with the shading removal to obtain the melanin, hemoglobin, and shading components.

Physiologically based image processing could be applied to the components to control the physiologically meaningful change of skin. The processed components are synthesized to obtain the image using E-cosmetic. Figure 5 shows the increase or decrease of the component homogeneously. Realistic change can be achieved by this method. Computer graphics technique can not be archived to this realistic change. This result shows the effectiveness of the image-based approach using computer vision technique.

4. Appearance reproduction for e-commerce [3]

It is important to reproduce equally perceptible images across different displays in the Internet shopping system. To solve the difference of color appearance between two displays, many studies have been done on the device independent color reproduction. However, a little has been studied on a device independent reproduction of glossiness of the object.

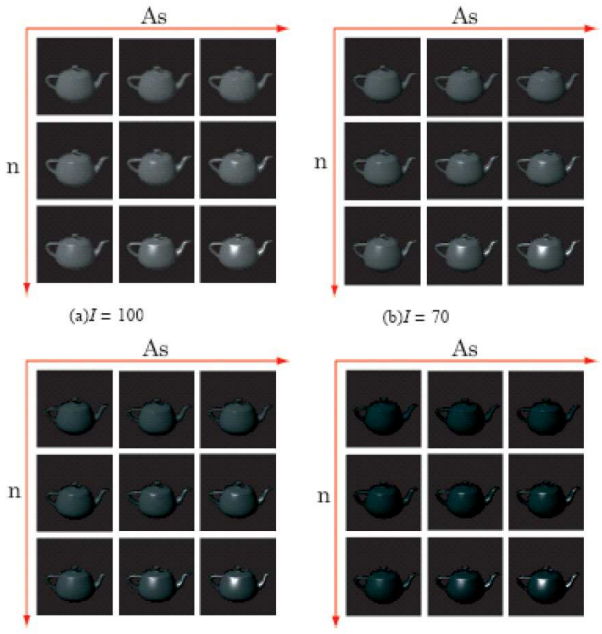

Figure 6: Images used to make the gloss model.

In the e-commerce system, the gloss reproduction is also important for customer. We developed the gloss reproduction system based on a perception of the human vision by using the various images of glossiness and luminance of display. Figure 6 show the images used to model the glossiness which is the function of luminance of display and parameters of BRDF on the object surface. The approach is based on the technique proposed by Ferwerda et. al [4] where glossiness is modelled under various diffuse reflectance of the object. Psychophysical scaling technique was introduced to clarify the relationship between the attribute of human gloss perception and the physical properties of the glossiness of the object in their paper.

Our developed model for glossiness is as follows.

$$G = 54.7\sqrt{A_s} + 4.1 \times 10^2\sqrt{n} + 5.4\sqrt{I} - 76.3 \quad (R^2 = 0.803)$$

where G is the glossiness value obtained by the subjective evaluation to the images shown in Figure 10, I is the simulated luminance of display in those images. As the parameters for BRDF, A_s is the power of specular components, n is an index that simulate the degree of imperfection of a surface in the Phong reflection model. It is noted that the simulated luminance I is introduced into our glossiness model.

The developed glossiness model is used for matching the gloss on different devices. As is written above, the model is written by parameter for BRDF on the surface and the luminance of the display. The luminance of the display may be pre-defined in color management system such as sRGB or ICC profile, or estimated by simple subjective evaluation on the display. Figure 7 shows an example of the isogloss curve, which is obtained based on the gloss model. By using this isogloss curve, glossiness of the object can be preserved in changing the luminance of the display.

Figure 8(a), (b) shows the images on high luminance display and low luminance display, respectively. The same data is displayed on each device, although the appearance of gloss looks different. Figure 8(c) shows the image compensated along the isogloss contour by keeping the luminance in Figure 8(b). By using images along the contour, we can produce images with same glossiness on different displays.

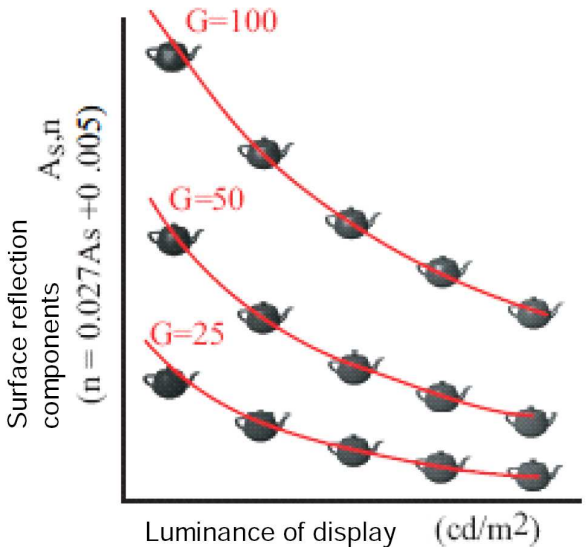

Figure 7: Iso-gloss contours.

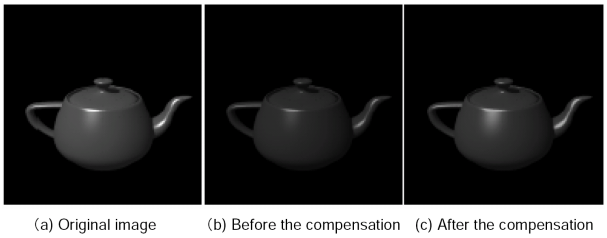

Figure 8: Device independent gloss reproduction based on the iso-gloss contours.

4. Conclusion

The case studies for appearance reproduction were introduced based on the our previous research for 3D color proof system, image-based skin analysis and synthesis system, device independent gloss reproduction system. These case studies showed the effectiveness of appearance reproduction in the product development. It is noted that this paper is written based a part of my review in Color Research and Application [1].

References

[1] Norimichi Tsumura, Appearance reproduction and multi-spectral imaging, Color Research and Application Vol. 31, No. 4pp. 270-277(2006)

[2] Ishii T, Tsumura N, Shishikura M., Miyake Y., Reproducing 3D Prints on Monitor by Relative-Glossiness Matching Technique, IS&T/SID's 11th Color Imaging Conference, Color Science, Systems and Appl. , 23-29(2003).

[3] Tsumura N, Ojima N, et al, Image-based skin color and texture analysis/synthesis by extracting hemoglobin and melanin information in the skin, acm Transactions on Graphics, 22:770-779(2003).

[4] Ikeda T, Tsumura N, and Miyake Y. Device Independent Gloss Reproduction Model for E-Commerce: Estimation of Radiance on Display, Proc. IS&T PICS Conference,:425-428(2003).

[5] James A. Ferwerda et al. : "A psychophysically based model of surface gloss perception.", Proc. SPIE Human Vision and Electronic Imaging IV, 291-301 (2001).

Biography

Norimichi Tsumura was born in Wakayama, Japan, on 3 April 1967. He received the B.E., M.E. and Dr. Eng degrees in applied physics from Osaka University in 1990, 1992 and 1995, respectively. He moved to the Department of Information and Computer Sciences, Chiba University in April 1995, as an assistant professor. He was a visiting scientist in University of Rochester from March 1999 to January 2000. He is currently associate professor in Department of Information and Image Sciences, Chiba University since February 2002, also a researcher in PRESTO, Japan Science and Technology Corporation (JST) since December 2001. He got the Optics Prize for Young Scientists (The Optical Society of Japan) in 1995, Applied Optics Prize for the excellent research and presentation (The Japan Society of Applied Optics) in 2000, Charles E. Ives Award (Journal Award: IS&T) in 2002. He is interested in the color image processing, computer vision, computer graphics and biomedical optics.

Invited Lectures

The response of primate cone-opponent cells to light stimulation

Thorstein Seim and Arne Valberg
Norwegian University of Science and Technology, Section of Biophysics and Medical Technology, N-7491 Trondheim, Norway

Cone-opponent cells are found at several levels of the primate visual system. Of the six main opponent cell types in the retina and lateral geniculate nucleus (LGN), two parvocellular cell types (the Increment and Decrement cells; also called ON and OFF cells) are devoted to the L-M dimension of cone space while two other I- and D-cells deal with the M-L dimension. Two other cell types combine S-cones with a sum of L and M-cones (the bistratified "Blue ON cells" and the much rarer "Yellow ON cells"). These six cell types show a characteristic response when the retina is exposed to stimuli of different wavelengths and intensity (luminance), and this behaviour has, for a fixed stimulus size, been modelled by an opponent combination of cone signals to retinal ganglion cells. These signals were computed by a linear combination of familiar hyperbolic functions describing the dependence of cone potentials on light intensity. These hyperbolic functions represented the only non-linear stage of the model. We have earlier demonstrated how subtracting the response to achromatic stimuli separates out a chromatic component that allows for the scaling of chromatic colour differences (Valberg et al., JOSA, A3, 1726-1734, 1985). Here we present additional data on how such cells respond to stimuli varying in wavelength, luminance, and size. It is shown how a combined activity of 'L-M' and 'M-L' types of Increment parvocellular cells largely cancels the chromatic component in the response and amplifies the response to bright achromatic stimuli. The same applies to 'L-M' and 'M-L' Decrement cells and dark achromatic stimuli. We also use the experimental data to determine spatial sensitivities of the receptive fields of the opponent cells. Combined with area responses, the model is used to predict the spatial structure of excitation and inhibition within the receptive field. The result is related to the spatial distribution of cone types within the excitatory and inhibitory areas and a possible overlap of excitation and inhibition, like in the "Mexican hat" model.

Recent developments in ICC colour management

Phil Green
London College of Communication, pj.green@lcc.arts.ac.uk

Initially conceived as a static file format to encapsulate colour transforms in a form that is interoperable and produces consistent output, the ICC specification has recently undergone amendment that significantly extends its capabilities.

Version 4 of the specification was published some years ago, and resolves some of the earlier ambiguities in the specification. Most colour management products now have the ability to make or use V4 profiles. However, the most important feature of V4 is only recently beginning to be realised. In the V2 architecture, input profiles map to the Profile Connection Space (a more or less unbounded CIELAB encoding with D50 illuminant), and output profiles map from this PCS into the device space. Where the input and output media have different colour gamuts, some form of gamut compression must be applied in this workflow, but neither profile knows the gamut of the other. This results in compromises being made which can severely restrict the gamut of the final reproduction. While this is not an issue for reproductions using the colorimetric intent, it leads to a loss of potential quality when using the Perceptual rendering intent. The Perceptual Reference Medium Gamut was adopted to address this problem by having a well-defined colour gamut for data in the PCS. We consider here how the PRMG is used in a colour reproduction workflow, and we report the development of a profile which maps between the PRMG and the sRGB colour spacefor the purpose of display viewing.

The various flavours of PDF/X have become a major element of graphic arts workflows. In the most recently adopted version, the trend towards the inclusion of references to well-defined external resources is continued by providing a mechanism for referring to resources by their URL. One implication of this is that an ICC profile specified as the OutputIntent of a document may be given as a URL for the profile rather than including the profile in the document. This is expected to be particularly important for variable data printing where it is less practical to include profiles for each element of a variable data stream. The ICC has developed a Profile Registry where profile providers can register profiles based on standard characterization data sets, and which can then be referenced by a permanent URL based on either the profile name or its profileID value. The practical application of this in graphic arts workflows is considered, together with some reflection on the requirements of standard characterization data.

The ICC specification has previously defined an encoding range for CIELAB which limits L* to 100. This is highly approriate to graphic arts workflows where the reference white is taken as a diffuse white reflector. However, there is increasing interest in colour management in digital photography and the digital motion picture industry, where the scene adopted white may have a luminance well beyond that of a diffuse reflector. In such high dynamic range imaging, the requirement to compress or clip to the PCS encoding range can cause severe limitations on the processing possibilities, including re- purposing of data across different media. The recently adopted floating point proposal provides a significant extension to ICC capabilities by allowing headroom in the the encoding. This proposal also incorporates other important extensions, including the ability to use a floating point encoding for look-up tables, and the ability to add additional processing elements (beyond those already defined in the specification) in the profile. The use of such processing elements by a profile and a CMM makes it possible to generate dynamic, programmable transforms which can handle a much greater range of colour processing tasks than envisaged in the original ICC architecture.

Microsoft have recently released the Vista operating system which incorporates Windows Color System. Tis represents a significant extension to the capabilities of ICM 2, and like recent ICC developments, points in the direction of dynamic and programmable colour management. WCS is fully compatible with ICC V4, and is likely to increasingly be used by consumers on Windows PCs. We consider the implications for professional workflows, such as the possibility

of interoperability issues arising with customers supplying work with WCS profiles.

Inkjet in question: adapting current colour and ink technology for the requirements of the user

Carinna Parraman
Centre for Fine Print Research, University of the West of England, Bristol, BS3 2JT
Carinna.Parraman@uwe.ac.uk

"It is of interest that, regardless of the number of impressions, the inks may be selected solely on the basis of their color gamut. Their colors need not be cyan, magenta, and yellow; nor is it required that they be transparent. The way is therefore opened for entirely new printing processes." [Hardy and Wurzburg 1948]

Abstract

This paper is an overview on the current application of inkjet and it's, as to yet considered unfulfilled potential, which as a technology, is as revolutionary as Caxton's printing press; and a presentation of an approach to develop inkjet from the perspective of the user. The paper considers the impact of technology on the user, and vice versa, responses to how inkjet technology is being adapted. It highlights recent developments in pigmented inks and the introduction of new colours by the three major inkjet companies: Canon, Epson and HP. However the introduction of new colours might fulfil objectives to expand the printed colour gamut that is based on a photographic colour reproduction requirement, but does not address how the technology can be thoroughly developed as an entirely novel colour printing system. Inkjet is in a transitional phase from classic image reproduction towards 'creativity'. The presentation discusses the implications of the need to change methods in mixing inks that moves away from existing colour spaces, non intuitive colour mixing to bespoke inks sets, colour mixing approaches and colour management methods that are not reliant on RGB or CMYK.

Background

The current situation is how colour management systems, since the early 90s, have transformed the print industry in providing colour fidelity and colour consistency, which has brought together the wide range of print industries: newspaper, poster, fine art, photography, interior design, textiles; into working with a ubiquitous colour language. For industry, this management of colour has provided the commercial printer with a streamlined method of printing from workspace to printer to paper. Furthermore, print hardware and software has also become rationalised. However, industry has now begun to question what has been misplaced in exchange for commercial expediency? The industry has come to realise that although workflow methods are vital for commercial growth, there is a very large and significant other market, which belongs to the artists, designers and users. This research is undertaken from the perspective of the artist/designer/user.

Over recent years inkjet technology has developed at a pace, and has evolved as a sophisticated software and hardware tool for the reproduction of digital photographic images. As improvements continue in inkjet head technology, inks and colour gamut, thus the gap between the traditional photographic print and the inkjet print has narrowed. However, there is a growing requirement for the user to gain access to an inkjet technology that is not necessarily dependent on photographic printing, which might contain, for example fields of colour, fine lines, blends and text. These requirements could be gained through alternative print and colour management methods, such as the development of novel colour sets and modifications to print software and hardware.

The User

Frustrated by the hardware, organisations have been driven to desperate measures. As R. Mac Holbert described how, at Nash Editions, they invalidated their warranty on their 126,000 dollar

Iris (3047) printer by sawing off and raising the print heads to print on thicker paper (History of Nash Editions p.29). Or at the Centre for Fine Print Research University of the West of England (UWE) Bristol, we rewired the switches to isolate the paper path mechanism so that (thicker) papers could be accurately registered and reregistered for overprinting to increase the density of black; and as a matter of course, the need to lift or remove the lid from the printer in order to gain a better understanding of the inner mechanisms.

From the perspective as a printer and printmaker, and working collaboratively with artists, a common response to how a final printed image is obtained is through 'trial and error'[1]. Accurate gamut mapping from monitor to print is undermined by many unknowns: by non white paper, textured paper, large fields of printed colour that might perceptibly change according to scale, simultaneous contrast and metamerism. The processes and methods to achieve a high quality image, is more often hard won through progressive steps: the need to acquire tools and skills to make a competent image is one that evolves as the user becomes more familiar with the technology.

Furthermore, as a practitioner of fine printmaking, traditional printmaking is also used as benchmark for the digital printed image, and therefore the fine art and design sector might have different parameters for considering the quality of the finished image. An analysis of the work is based on an artist's conception of the work and a subjective assessment of print surface, colour and image quality, which although may appear to be based on the same criteria as a reproduction, the impact on the viewer is quite different.

User requirements for improving inks

With the emergence of digital imaging technologies in the 1980s so too was there a desire to print high quality colour images. Whilst Nash Editions recognised that the Iris technology produced beautiful rich and dense colour, they also quickly realised the dye based inks were incredibly fugitive. They found that the early inks, if left in daylight for a few hours would noticeably fade (Holbert, 2007, p.20). Similarly, in 1999, when we began working with an Encad Novajet, these inks were so fugitive that when printed on commercial coated papers, they could fade in a dark room overnight. As a way of addressing this problem, Lyson Inks responded to requirements by making fine art inks that would enable the user to obtain a compromise between colour permanence and brightness of colours, not as yet achievable in pigment inks.

The concern for permanence however motivated users, conservationists and representatives from the paper and packaging group to address these problems, which have resulted in a series of ongoing conferences hosted by the Institute of Physics in London, to assess and debate the preservation and Conservation Issues Related to Digital Printing and Digital Photography (2001 onwards).

Since 2000, developments in inkjet ink technology has significantly changed from when inkjets used dye-based colour inks and pigment-based black, these are still used in the smaller deskjets, small molecule dyes are used to capitalise on the wider colour gamut. However the trend is to move towards pigment based inks which are resistant to UV and gas fading, and because they are more complex, break down slower than dyes. As advances are made in inkjet ink technology their brightness has improved, resulting in the majority of wideformat printer manufacturers using pigment inks. This is evolved as a user demand for archiving and colour longevity, in terms of intended application of large print works: exhibition, display and fine art and poster market.

For the medium and wideformat market, eight-ink sets and twelve-ink sets are becoming ubiquitous. Canon's LUCIA Pigment Ink Technology contains twelve-colour pigments using red, blue, green, grey, photo grey, cyan, photo cyan, magenta, photo magenta, yellow, (regular) black,

[1] In response to a questionnaire given to 20 artists as part of a background to an exhibition entitled 20:20 A documentation of Artists making prints. http://amd.uwe.ac.uk/cfpr/index.asp?pageid=1378

and matte black. The VIVERA range of colours introduced by HP through the new Design Jet Z series includes light grey, grey, matte black and photo black, magenta, yellow, cyan, orange/red, blue, green, light magenta, gloss. With the inclusion of green has resulted in the light cyan being redundant.

For the black and white reproduction, Epson's UltraChrome K3 eight-colour set includes two different black ink modes - photo black and matte black; Canon differentiates between matte black, regular black, grey and photo grey, which according to Canon, the combination of grey and photo grey enables smoother transitions from light to dark. HP have included four grey/blacks, with the addition of a gloss, which as part of their media profiling management system can be switched on or off to enhance density or is an automatic component of gloss papers. It can not be used for matte papers.

Epson UltraChrome K3^{TM} ink incorporates a High-gloss Micro-crystal Encapsulation, which according to Epson literature, each pigment is coated in a resin, which reduces the grouping of pigment particles. This is similar to Hewlett Packard's Vivera Electrosteric Encaplsulation Technology or EET; negative electrostatic charges within the resin layer, which coats the pigments and prevents pigments from grouping together or repels each pigment particle.

Mixing colour

For traditional artists working in colour, their ability to layer colour onto canvas or paper with the objective to 'imitate nature' through colour, light and dark, and texture is demonstrated through traditional easel painting and printmaking. For the photographer, the process of creating a coloured photograph, is a very different activity and requires the mixing of light wavelengths to create an image. Furthermore for the digital printer, software applications are based on less intuitive colour methods of mixing: red, blue and green (RGB), mixing colours additively or cyan, magenta, yellow and black (CMYK) which are based on printer's process colours. However, explanations on how colours are converted, for example, in the digital imaging pipeline are often confused.

There has seen a shift in the recent printer manufacturers from CMYK printer drivers to RGB, this closely mirrors the perceived drive towards the photographic market in maintaining a clear relationship between traditional photographic red, green and blue filters, monitor colour. However anyone attempting to mix a colour will quickly realise that, at least working in a CMYK space a better idea can be obtained by, for example, mixing 100% Magenta, with 60% cyan, with 30% black will create a purple. However how might the same colour be achieved using RGB? (Red:72 Green:30 Blue: 86). Both colour-mixing methods do not enable a meaningful method of mixing colour.

How might inkjet be developed?

As a way of illustrating how inkjet might be modified, one can draw upon the technological parallels of Screenprint or Serigraphy and how this process can be used as a benchmark for inkjet. Since the advent of screenprint, at its most utilised in the 60s and 70s when photosensitive coatings were introduced, the artist was able to combine text, photomechanical image and hand made marks in a highly innovative way. This enabled the artist to over-layer colours, employ light over dark, opaque inks and translucent inks, gloss and matt varnishes and build up layers. Although the mesh size of the screen reduced the possibility of high quality or continuous tone images, the artist however was able to compensate by employing a variety of means to create highly saturated colour images through stochastic halftoning, multi coloured, blended or flat coloured, multilayered image making and printing.

In both instances, screenprint and inkjet have good and problematic aspects to the technology. The following list highlights these pros and cons:

Inkjet and screenprint - pros and cons

Screenprint: Pros:

- Hands on: paint mixing by hand, control over colours
- Wide range of colours, including basic CMYK
- Can control chronology of colours and layers
- Surface topology and texture, optical qualities – can see 'through' layers.
- Using translucent inks increase density.
- Mixing inks from a transparent base and/or mixing colour from an opaque base

Cons:

- Limited resolution, for photomechanical reproduction, can see the dots, not wholly photographic or continuous tone.
- Requires an understanding of the process ie. viscosity of ink, squeegie pressure and angle.
- One screen for every colour
- Messy, requires cleaning

Inkjet: Pros :

- Increasingly, a closed loop system (Photosmart), non expert can print and obtain quality images
- Colours are entirely translucent, can print in any order, colours are designed to mix together
- Colours are highly saturated, provide a colour gamut suitable for photographic reproduction
- Small and medium sized dots, drop on demand technology, that can provide almost continuous tone resolution
- Incredibly detailed – produce a high detail and fine continuous lines – not possible by any other process

Cons:

- Limited control over printer and workflow
- Colours limited to photographic reproduction – RGB, CMYK, LAB
- One pass, surface uniform, no surface topology
- Cannot (easily) modify colours,
- No opaque colours, no gloss or matt.
- Cannot separate channels
- Exact registration problematic – hit and miss

Developing inkjet for the 'Creative'

To generate an image, the artist could combine both photographic images and flat colours, or choose just flat or blended rendering. In any situation the user would have a range of choices, and that would extend the potential of the inkjet hardware beyond photographic reproduction.

Basic components of the inkjet printer might comprise:

Re registration with fine tuning (sideways, backwards and forwards) Paper thickness sensor – heads might be raised or lowered to accommodate thicker papers Built in device for profiling Photosmart capability employing existing pigment inks 'Out of the Can' printer colours and software for mixing, printing flat colours and blends, shapes and fine lines.

Developing the idea of a novel RIP:

The following method of image production would apply to the printing of flat, blended areas of colour, with the intention to over-layer colour.

Working from software such as Illustrator or Photoshop, a series of layers would be generated – each layer representing a colour - similar to the way one would work as a printmaker. These could be soft-previewed with all the coloured layers as a composite, so as to give an indication of how the final printed image would appear. This would be done by ICC profiling. Experiments have already been undertaken using alternative colour ink system.

The development of a colour mixing system:

Using a colour system similar to an 'out of the can' approach – a range of 9 basic colours, ie. blue shade red; yellow shade red; red shade blue; green shade blue; green shade yellow; red shade yellow; black; opaque white; translucent white/gloss extender; that can be used at any percent (1-100%) to produce a range of hues, shades and tints.

Conclusion

Over the last ten years the impact, the evolution and the relationship with emerging digital print technologies has been one of grappling with a hardware and software that, as yet, has not achieved its true potential: the inkjet print is still evolving.

A Generalized Approach of Color Morphology by Means of Pareto-set Theory

Mario Köppen
Faculty of Artificial Intelligence Kyushu Institute of Technology, Fukuoka, Japan
mkoeppen@ieee.org

Katrin Franke
Norwegian Information Security Laboratory (NISlab), Gjøvik, Norway kyfranke@ieee.org

There is no unique way to extend the concepts of gray-scale morphology to color images. Different viewpoints have led so far to the proposal of a number of useful operations for the processing of color images. Among these viewpoints we can find the linear weighted, or scalar, approaches, where vc is mapped onto P by a scalar function that is monotone in each argument. Then, standard gray-scale morphology can be applied to such transformed images IP. A typical choice in the RGB color space is the sum of the R, G and B intensities. Then, the color dilation just reads as selecting criteria the color value with the largest sum from each pixel's neighborhood.

More refined concepts have been based on the use of fuzzy-fusion measures, including the proposal of a color morphology that cannot effectively be reduced to a linear weighting approach. However, most of these approaches are considering the extension to color morphology as an extension of the selection criteria, instead of an extension to the handling of multiple intensities.

Thus, we were studying an intensity-based color morphology, with its main difference to other color morphologies being the generation of a gray-scale image that cannot be the result of a morphological operation on a grayscaled version of the color image itself.

The formal techniques for achieving this goal came from the field of multi-objective optimization and its related concept of Pareto dominance. A consideration of the various Pareto-set-based means and techniques that have been developed in the past for the study of (continuous) multi-objective optimization problems lead to the formulation of a number of image-processing operators. A simple example is the generation of a gray-scale image from a color image, where each pixel's gray-value represents the number of Pareto-dominating points in the neighborhood of this pixel. Practically this comes out to be an edge operator.

In this talk the usage of Pareto sets for image-processing operators will be discussed in detail, and some potential applications of this approach to color morphology will be shown.a multi-variate channel-intensitiy vector

Submitted Papers

Digital Camera RAW profiling

Jack Bingham and Derrick Brown
Integrated Color Corporation – Billerica, Massachusetts

Jo S. Kirkenær
JSK Consulting – Carlsbad, California

Introduction

Raw camera files are considered by many to be the digital equivalent of the unprocessed photographic negative. It does not offer the kind of exposure latitude we expect from negative film, but in many other aspects it holds true.1 To yield a good visual image, the RAW file has to be processed and rendered to an RGB color space, generally sRGB or Adobe RGB (1998), and if you've ever experienced color mismatch between the printer and your monitor, or have been confused by RAW file formats and ICC profiling and not getting the best results from your digital camera and printer, this paper will detail solutions to deal with Raw camera files and how to properly profile the digital camera. With an understanding of how to manage photographic color, you can solve these problems. When the camera produces images using the standard color encodings it is performing a color rendering and when you then try to generate a profile for this condition by photographing a target, you are actually profiling the rendering and the results will generally be sub-optimal, because the profile now will try to undo the color rendering in the camera. This paper addresses the use of ICC profiles in workflows that start with Raw camera images, including coordination of camera settings, RAW processing, and ICC color management. The new capabilities of ICC version 4 profiles will be discussed, including the use of the re-defined perceptual rendering intent with output-referred, scene-referred, and raw camera files. Rather than using default custom profiles to render the RAW data to match the scene or create a pleasing reproduction of the scene on the printed paper, we will develop a process and generate a single profile for the specific camera, putting an end to the myth that you need multiple profiles for different imaging conditions such as daylight, shade, tungsten & fluorescent adopted white.

Photographers know that the world we view is difficult to record on film, and just as difficult with a digital camera. What if we could capture all the color and tone that we can see with our eyes with our digital camera? No need for fill-flash or additional lighting. This is, of course, not possible. A scene generally will have a huge dynamic range the tones from dark shadow to bright highlight may be as much as 10,000:1. A corresponding print will only cover a dynamic range of about 200:12, while a good display may give us as much as 1,000:1. So the digital camera will "see" and record the world quite differently from how we see the world. The initial RAW data has to be rendered in an attempt to match the scene as best as it can, or it can be rendered to create a pleasing reproduction of the scene. There is big difference between the two, and the methods and technology described in the paper will try to shed some light on these differences and the use of ICC profiles to accomplish the desired results. Since we have to view the digital image on something, we have to select a rendering for display or print. Films have always included built-in contrast and colorfulness boosts with highlight compression, to make pictures look better.

If we refer to the measured scene color as the camera captured it, we deal with the Scene-Referred image. But we need to view it either on a display or on a print, hence we need to make the image look pleasing and produce the desired color appearance the photographer wishes to express and reproduce and now we have rendered the image as Output-Referred. Most cameras, particularly consumer type point-andshoot cameras perform this rendering automatically to an image encoding of sRGB or Adobe RGB (1998). Advanced consumer cameras and professional cameras usually have a selectable rendering, but in RAW mode this rendering becomes the job

of the image creator, usually the photographer, and this is where we can get some help from a custom ICC profile.

It should also be noted here that two sRGB encodings of the same scene from different camera brands should match, but that is rarely the case. The match is no closer than two shots of the same scene on two different types of film. However, using ICC profiles different cameras can be made to reproduce the same scene in almost the same way.

Using RAW format gives us the opportunity to create custom profiles and working with at least 12 bits per channel. Using a default RAW translator will still render and encode a default profile such as sRGB or Adobe RGB (1998), or other pre-set profile used as the Working Space in Photoshop, such as ProPhoto (ROMM) RGB. It should be noted that sRGB represents as a reference medium a standard CRT display, while with ProPhoto the reference medium is the ICC perceptual intent reference medium reflection print3. The Adobe RGB reference medium is currently not clearly defined, but will most likely reference a viewing condition of about 160 to 200 lux at Daylight D65 white point, viewed in a dim surround. However, setting a custom profile will give a much better rendering and keep all the colors and color differences that the camera actually recorded.

Different profiling packages uses different targets, from the most photographed target of all times, the MacBeth ColorChecker to the IT8/7-1 and IT8/7-2, mostly for use with scanners, to custom targets tailored to the desired scene. It is also important that the target includes checks for luminance uniformity as in the Digital ColorChecker and ColorEyes 20/20 targets. The drawback with most targets is that they only represent a small portion of all the colors available in the original scene, and in some cases would be restricted to specific colors in photographic paper, hence possibly restricting the overall resulting gamut.

It has been general practice and demonstrated multiple times 4 5 that in a fixed environment such as a photo studio or a copy stand for fine art reproduction the camera and imaging condition lend itself perfectly to proper characterization and ICC profiling. It is when the camera is taken out into the "Real World" where current thought is that multiple custom profiles are needed, or just using standard color space profiles.

The perceptual intent of these true camera profiles should include color rendering to the ICC perceptual intent reference medium and should be used for general photography, while custom camera profiles will typically be specific to particular shooting conditions. The colorimetric rendering intent is generally fixed to give the most accurate, though not necessarily most pleasing, rendering of the scene, while the perceptual rendering intent can be manipulated and tweaked to give the most pleasing, yet not necessarily accurate rendering of the scene. But with a profile and the images captured under the same condition, the results will be consistent and good, and very little further processing will be required, at least as color is concerned.

In this paper we will show examples and comparisons of various standard profiles compared to both display and print profiles, as well as custom profile comparison to standard RGB profiles and color spaces. This paper will not discuss the virtues of the different profiling packages and targets, though this could be a worthy student project.

Process

Before we start with the profiling process it is critical to understand the sensitivity inherent in the digital camera. A color variation from one light source to another of 50 points Kelvin is very apparent. That means the following: Any influence reflected on the target other than one main light is more than likely to alter the data. Two softboxes of slightly different ages will have different color nylon diffusers. Two flashtubes of different ages will discolor differently, not to mention any filtration dome over the tubes. On location any of the surroundings could reflect on the target, degrading the data. Setting the target on a colored seamless background in studio will reflect color up into the bottom of the target more than the top. This discussion about having

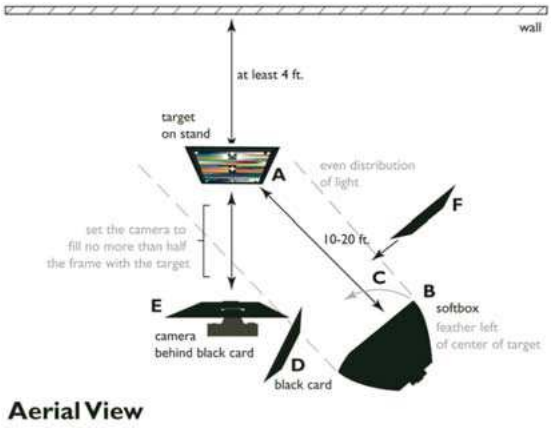

Figure 1: Target setup

to profile scenes is a direct result of trying to profile scenes. By doing this you automatically introduce variables in the data that only exist in that scene, thereby being trapped into profiling every unique scene.

The process that works to create a universal profile requires a different approach. In order to get the most accurate data from the target we need to eliminate as many variables as possible. Lighting is the most critical. Since there are too many variables with two lights, softboxes, strobe tubes, power packs all of which can not be accurately tuned into a matched pair we should rule that approach out from the start. Now it is possible using tungsten lights, dimmers and a color meter that one could tune a pair of lights to be extremely close in color temperature. However the likelihood of the average user not only having the tools to do this, but going to the trouble is highly unlikely. So the only real alternative is one light. It then no longer matters what the conditions of the diffuser, the tube or the cover are. This is shown in Figure 1.

Now of course we introduce a problem that two lights in a copy setup is designed to handle with ease. The target now has more light on one side than the other. By carefully following the diagram shown here one can gradually "cut" the light on the bright side of the target until the left and right sides match. Note that the photographer accustomed to shooting copywork will pull out the incident meter and use it to balance the light across the target. Since the digital camera is sensitive well beyond the 1/10 stop range of a light meter this approach can not work. However we have a much more accurate tool in our hands; measurements taken in Photoshop can provide the necessary accuracy.

Once the target is even, and using the Coloreyes 20/20 target as an example, shown in Figure 2, it provides four white corner patches from which to take measurements, as shown in the figure. It is important to match the exposure of the target to the actual luminance values within the target to avoid adding any exposure compensation into the profile. The white patches on the ColorEyes target are between an L or 92 and 93, so by using Photoshop to measure the corners and adjust exposure accordingly the data is closer to the original.

Finally, gray balance is critical. Like linearizing a printer before profiling, the camera must be linearized to the lighting condition. Auto will not work here. Once the target parameters are achieved, the process to build a profile is simple. Coloreyes introduces one extra variable here that is critical. When building the final profile the user can choose between a profile that adjusts lightness, chroma and hue or just chroma and hue. On the surface it would seem that we want the most accurate profile we can build. In reality by allowing the profile to adjust lightness we introduce another problem. Cameras do not produce data that represents a scene accurately. They are actually tuned to adjust the contrast range to something we have come to like rather than what would be an accurate rendering of the tonal range of the scene. So by allowing the profiler to adjust tonal values we end up with two problems. First the profile adjusts tones that

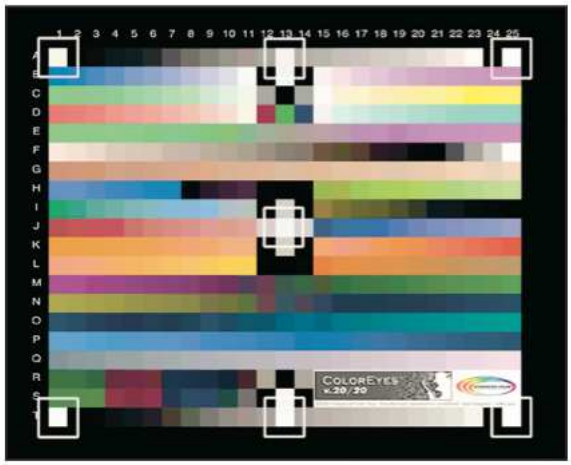

Figure 2: ColorEyes 20/20 target

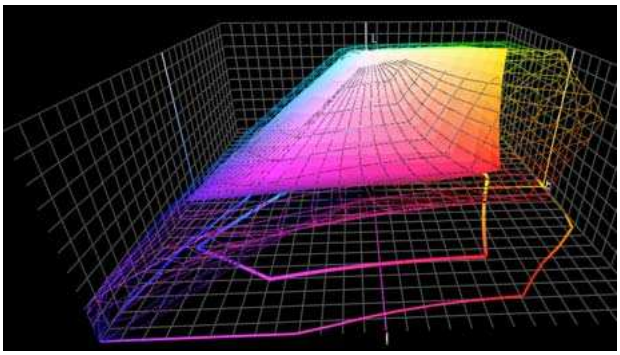

Figure 3: Custom Camera profile comparison.

it is inherently not designed to do. And the worst part is that the bulk of the adjustments take place in darker values where noise is present. Raw converters are designed to handle shadow detail and noise very well. Profiles are not. The second problem is that we generate a profile that every user will complain about being too flat. The tonal values will indeed be more accurate but that is not what the photographer really wants. The photographer wants a rendering of the scene closer to what the camera is tuned to produce.

So why does this create a universal profile? Profiling scenes introduces variables in the target that exist only in a particular scene. A profile made under these conditions will indeed be scene specific. By eliminating as many variables as possible we have much more accurate data about exactly what the camera can see. Now the final piece of the puzzle is making this profile work under different lighting conditions. The big conflict about this seems to be the suggestion that a camera behaves differently under different lighting conditions. While technically this might be true, from a practical standpoint it is clearly not enough of an issue to prevent a camera profile from working extremely well under varied conditions, and working better than Camera RAW processing or default profiles.

Back to the point about printer linearization; when we change ink we can run a linearization to update the profile. Gray balance is the same approach. By linearizing a camera to a given lighting condition the profile becomes valid for that condition.

Figure 3 shows the custom camera profile gamut compared with an sRGB default camera profile. The custom profile is shown as a wireframe. Note the significantly larger color gamut the camera is able to produce, that would just be clipped if using sRGB.

Example color pictures showing the differences between the best Camera RAW processing

Figure 4: RAW processing, outdoor scene.

Figure 5: Custom profile, outdoor scene.

and a custom profile are shown in the following figures. In Figure 4 the yellow flowers are saturated and blown out, while in Figure 5, each flower is clearly visible. Similar differences can be seen in Figures 6 and 7, where the custom profile gives better fleshtone and a better modulation of the overall lighting.

Conclusions

We have demonstrated that by treating the digital camera similarly to a scanner or printer by performing a white balance linearization, a single camera profile will render the RAW information to the most accurate as well as pleasing RGB data for presentation on a calibrated and profiled computer display or a printer in an ICC workflow.

References

[1] Bruce Fraser: "Real World Camera Raw with Adobe Photoshop CS2", Peachpit Press 2005.

[2] ICC White Paper 20: "Digital Photography color management basics".

[3] ICC White Paper 17: "Using ICC profiles with digital camera images".

[4] U. Lenz et al.: "Digital Camera Color Calibration and Characterisation", The Fourth IS&T/SID Color Imaging Conference: Color Science, Systems and Applications, pp 23–24.

Figure 6: RAW processing, person.

Figure 7: Custom profile, person.

[5] Lindsay MacDonald et al.: “Colour Characterization of a High-Resolution Digital Camera”, CGIV 2002: The First European Conference on Colour Graphics, Imaging and Vision.

Measurement of colour on translucent material viewed by reflection

A. Sole and P. J. Green
London College of Communication, adityasole@gmail.com

Keywords: white sample backing, transmissive media

1. Introduction

In graphics and arts industry, colour is printed on transmissive materials like polyethylene, cellophane, etc which are usually viewed by reflection. It is therefore, more practical to measure reflectance against a backing material rather than transmittance. According to ISO 5 – 4 and ISO 13655, when measuring a colour stimulus using reflection geometry the sample should be backed by either a white or black backing material. For a highly transmissive (virtually transparent) material when measured with a black backing material, it is difficult to obtain useful measurement because of the show-through of the black backing. In this case it is convenient to use a white backing with a reflection density which conform to ISO 13655 and ISO 5 – 4 specifications for a white backing material. However, at present there is a lack of materials which are known to conform to these specifications and which are widely available.

The objectives of this project were as follows:

1. To make a recommendation of backing material to be used when measuring colour stimuli printed on transmissive media with reflection mode geometry.

2. To develop a colour measurement procedure to make measurements relative to perfect diffuser.

3. To define a procedure that supports sharing of measurement data between organisations.

4. To test the colour measurement procedure colorimetrically and psychophysically

5. To develop a model to predict CIE XYZ tri-stimulus values of a colour patch to be printed on paper to match with the same colour patch printed on translucent substrate viewed by reflection with a backing material.

2 Methods and results

2.1 Recommendation of white backing material

Three types of widely available paper materials were considered, along with PTFE reference tiles of 10mm and 6mm thickness. All were checked for the conformance with the specifications for a white backing material given in ISO/CD 13655:2006.and CGATS/STF N 045. Table 1 shows the result.

It can be seen from Table 1 that none of the materials evaluated conform to all the requirements of ISO/CD 13655:2006. By using a double thickness the proofing papers meet the CGATS opacity requirement, but none of the papers tested met the ISO/CD 13655:2006 requirement regarding fluorescence. Hence there remains a need to either identify suitable materials for white sample backing, or to develop procedures that will allow a wider range of materials to be used.

Backing material	CGATS opacity	ISO 13655 reflectance	ISO 13655		Fluorescence	Diffuse reflectance
			L*	C*		
PTFE 10mm	✓	✓	×	✓	✓	✓
PTFE 6mm	✓	✓	×	✓	✓	✓
Proofing paper 1 (220gsm)	×	✓	✓	×	×	✓
Proofing paper 2 (240sgm)	×	✓	✓	×	×	✓
Office paper (280gsm)	✓	✓	✓	×	×	✓
Proofing paper 1 double thickness	✓	✓	✓	×	×	✓
Proofing paper 2 double thickness	✓	✓	✓	×	×	✓

Table 1: Comparison of the backing materials for the conformation to CGATS and ISO 13655 specifications

2.2 Procedure that supports sharing of data between different organisations

For data to be exchanged between different organisations, measurements made using different paper backing materials were made relative to reference backing material. The measurement procedure is based on the concept that the measurement made on the candidate backing material can be normalised to the reference backing material. Figure 1 shows the reflectance of two colour patches measured with PTFE as reference backing material and with candidate backing materials made relative to PTFE, and it can be seen that there is good agreement between the PTFE-backed and normalised reflectance

2.3 Procedure to make measurements relative to perfect diffuser

Measurements made relative to a reference backing material were also normalised to a perfect reflecting diffuser. The performance of this procedure was evaluated by comparing the reflectance curves of the measurement of colour patches made on reference backing material made relative to perfect diffuser and that measured on the candidate backing material made relative to perfect diffuser. Figure 2 shows the comparison of the reflectance curves of two colour patches.

2.4 Testing the procedure colorimetrically and development of the model to predict CIE XYZ tri-stimulus values

Halftone colour patches from two gravure prints on polyester of different opacities were selected and measured using the reference and candidate backing material. The reflectance measurements are made relative to a perfect diffuser by applying the procedure. Figure 3 shows the reflectance curves of the measurement of the colour patches made with candidate backing material made relative to a perfect diffuser and those made with reference backing material made relative to a perfect diffuser.

The reflectance curves for the colour patches coincide reasonably well.

A model was developed to predict the CIE XYZ tristimulus values of a colour patch to be printed on paper to match with the same colour patch printed on translucent substrates viewed by reflection with the double-thickness Proofing Paper 2. A matching experiment was performed to determine this relationship.

A greyscale printed on two polyester substrates and a paper substrate was measured using the double-thickness Proofing Paper 2. The reflectance measurements made on the polyester

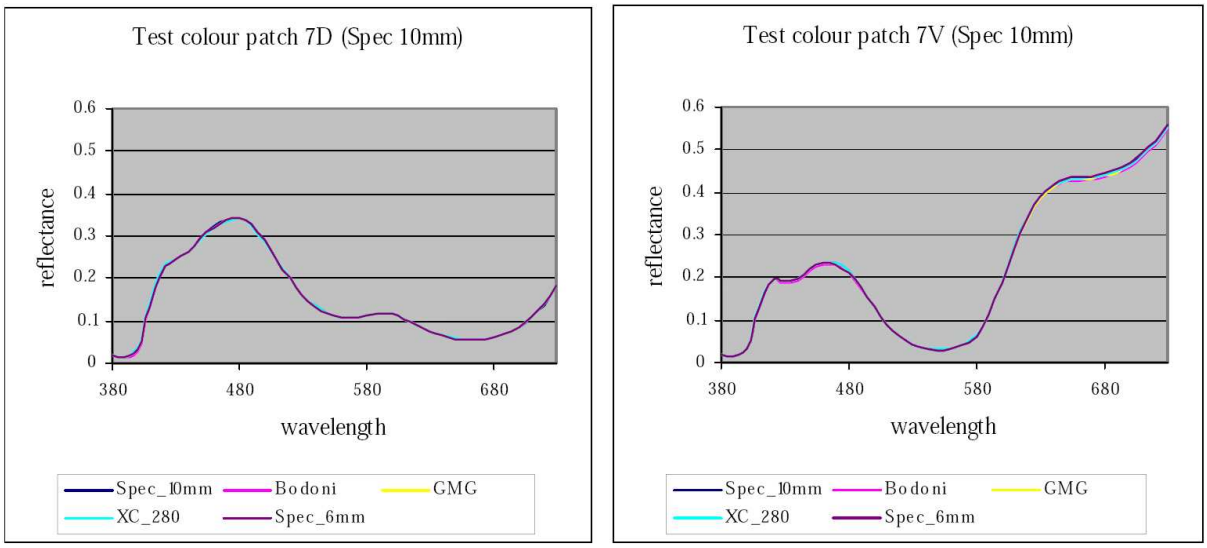

Figure 1: Comparison of reflectance curves measured on PTFE backing and measured on other paper backing made relative to PTFE backing.

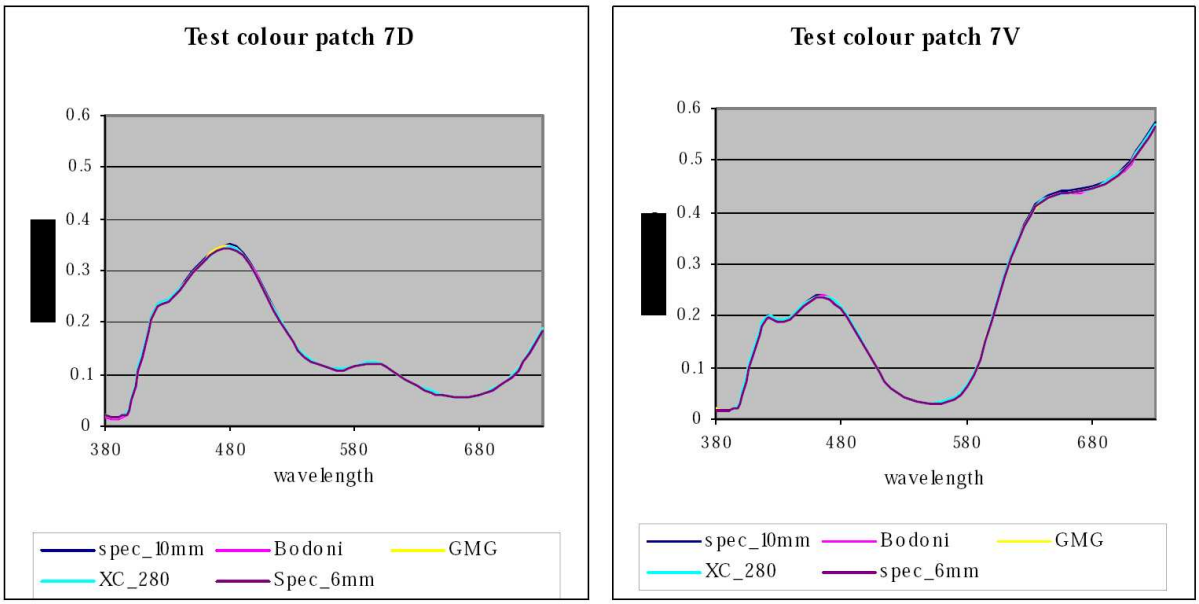

Figure 2: Comparison of reflectance curves measured on PTFE backing made relative to perfect diffuser and measured on other paper backing made relative to PTFE backing made relative to perfect diffuser.

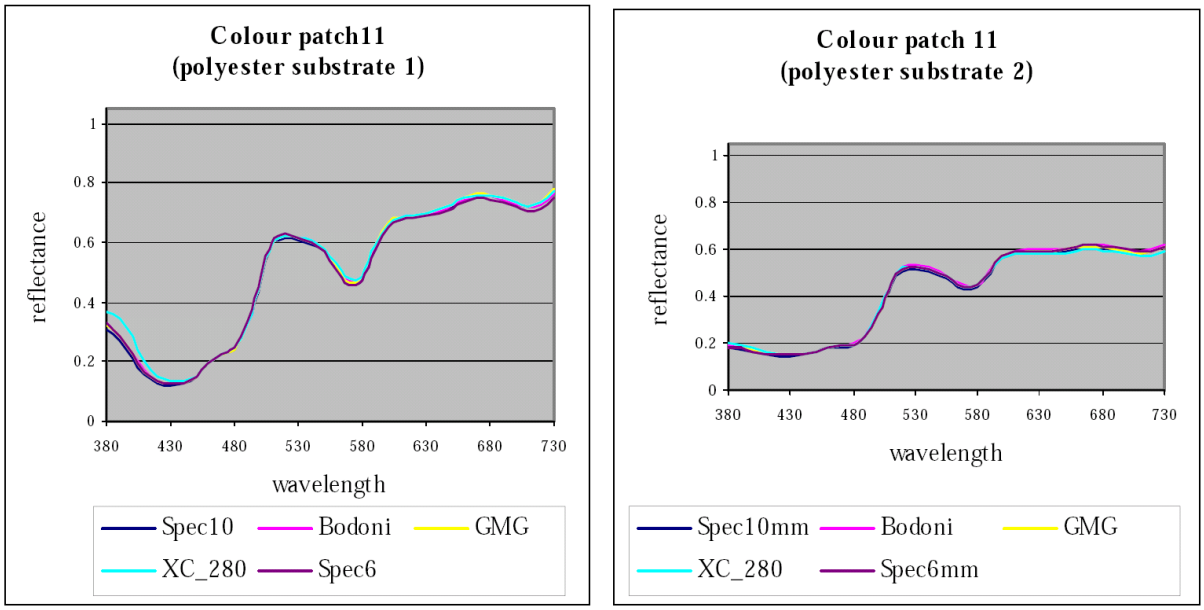

Figure 3: Comparison of reflectance curves measured on PTFE backing made relative to perfect diffuser and measured on other paper backing made relative to PTFE backing made relative to perfect diffuser

substrates were made relative to perfect diffuser as described above, and CIE XYZ values were calculated from these measurements. In the psychophysical experiment observers were asked to match the greyscale patches printed on the two white-backed polyester substrates to greyscale patches printed on the paper substrate, and the geometric mean of the visual matches was calculated.

The data measured on both the translucent substrates was combined and a single model equation was derived for both the substrates. Figure 4 shows the combined CIE Y tristimulus data with a trend line and the model equation.

This model was evaluated psychophysically using a halftone print of 10 colour patches and 33 colour patches imaged on Ekatachrome transparency. A category judgment technique was used for the experiment. Both the test prints were measured and corrected using the procedure described above to make them relative to perfect diffuser. The matching CIE XYZ values were predicted and printed on Kodak photo print 190 gsm glossy paper.

The reproductions were evaluated psychophysically by presenting these printed reproductions together with the transmissive samples on a white backing in a category judgement experiment. The results indicated that this model performed well for the halftone print and reasonably well for the Kodak transparency print.

3. Conclusions

1. None of the paper materials evaluated met all the requirements of ISO/CD 13655:2006,
2. A measurement procedure was developed to make white-backed reflectance measurements of transmissive media relative to a perfect diffuser. Proofing Paper 2 (used double thickness) performed best when using this procedure. Many similar materials would be acceptable for industrial use using this procedure.
3. A model was developed to match colours between prints made on white-backed transmissive materials and opaque materials. This model gave a good performance.

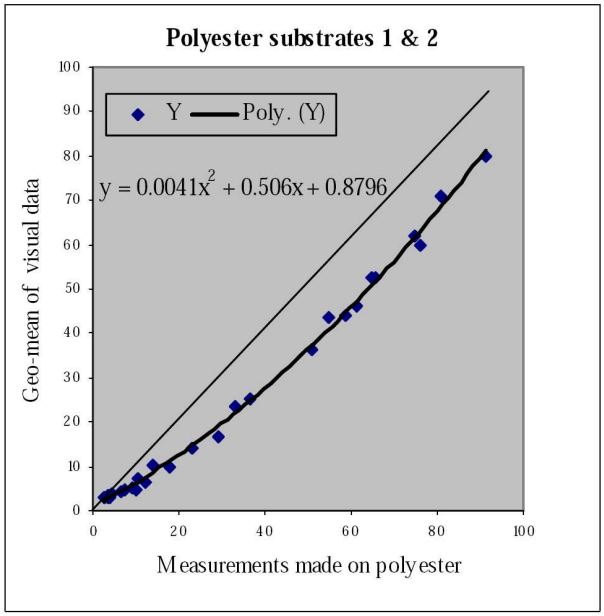

Figure 4: CIE Y tri-stimulus data with the fitting curve and the model equation.

Certifying Monitor Proofing Systems

Jo S. Kirkenær
JSK Consulting – Carlsbad, California

Introduction

In the US, the main printing standard to be met by printers is SWOP (Standard for Web Offset Publishing). Over the last decade ink-jet proofing systems have proliferated claiming to match the presses at this printing standard through the use of ICC profiles, and over the last couple of years color accurate soft proofing, also referred to as monitor proofing has made inroads into the proofing market.

Printers always looked to the SWOP certifying body to help sort out all the proofing systems, and through a process of visually judging prints, and measuring target patches, these proofing systems became certified for SWOP printing. With the ability to embed ICC profiles for other printing standards, or reference printing conditions, these ink-jet proofing systems could also be used to simulate and match these conditions.

The proof is considered the prototype of the printed image and as such, is a predictor of the many millions of copies that subsequently may be produced [1] it is critical that the proofing system is a reliable and consistent predictor of the actual process. Initially this was very subjective; a panel of observers compared reference press sheets to the proof sheet under controlled lighting conditions, and when monitor proofing entered the market, the same conditions and parameters applied here, though now the display itself was the canvas by the adoption of color management system software and by the adoption of device independent color variables [2].

Integrated Color Solutions (ICS), Inc was the first company to take their Remote Director software and an Apple Cinema display to SWOP and get it certified as a valid match between the rendered image on the display and the corresponding SWOP reference press sheet. Other companies followed suit as well. But the process was still very subjective, and two systems, both certified and placed side by side, could show more variability and mis-match than what most hard-copy proofing systems would.

At the 3rd Annual IPA Color Proofing RoundUP for 2005 [3] hardcopy systems proved very consistent both visually and numerically and monitor proofing systems proved that they could carry their own weight. Visual scores for monitor proofing were right in with the corresponding visual scores for the hard copy systems, under the same evaluation procedures.

In 2006 at the Annual IPA Color Proofing RoundUP hard copy and soft copy proofing systems were treated the same way, all participants were handed a printed characterization target, and told to make a profile and match the press sheet numerically. Only the judges had access to the visual part of the press sheet for final evaluation.

Though possible on some systems, the monitor proofing systems were not subjected to the Delta-E test [4], for reasons I will discuss later.

However, since the monitor proofing systems are able to accurately display colors on screen, this triggered a discussion to automate the process of certifying these systems for SWOP, or other reference print condition by removing the subjective factor and using metrological data.

In theory at least, rendering a color on the display through a color managed workflow and measuring that rendered color on a calibrated display should yield the same color within a very small DeltaE. This paper will show that this holds true and how this process can be used to certify displays to match a given printing condition.

In the initial phase of implementation, there will be a visual inspection prior to the metrological evaluation, primarily to save time by weeding out systems that clearly don't meet the standards.

Process

Since the spectral power distribution of the display is usually quite different from that of the viewing booth it may be necessary to apply a color appearance model when displaying the image on the computer. Even the white points, though both measured out to a correlated color temperature of D50 may appear visually different without it. This is the reason why numerical delta-E measurements were not applied at the 2006 IPA shootout. Different metrics and CAMs to different viewing environments yielded different measurements off the display, and absolute delta-E comparisons to the reference data were large.

In the monitor proofing environment, the CMYK data is converted to display RGB as follows:

$$\text{CMYK} \rightarrow \text{PCS} \rightarrow \text{RGB}$$

through the A2B1 tag in the CMYK profile. PCS is the Profile Connection Space, generally L*a*b*. With the proper display calibration and profiling, this data can then be directly converted through the B2A0 tag of the display profile to display RGB, and if measured with a reference instrument the actual color L*a*b* can be recorded. This recorded L*a*b* value can then be directly compared to the reference file that created the printing CMYK profile in the first place and any errors are then calculated and reported.

This is really no different from an ink-jet proofing system displaying a simulation of the press condition through the same A2B1 tag, but this time connecting with a CMYK output profile. The SWOP organization has already started a numeric certification program for hardcopy proofing systems, printing the simulated characterization target, and measuring the patches on this hard copy.

It should be noted that for the display measurements all the values of L*a*b* are to be calculated using the measured RGB white point of the display that is set by the monitor proofing system, the correlated D50 rather than an absolute D50. Hence the white point of the display should always measure L*a*b* = (100, 0, 0).

Even under these circumstances the most accurate reproduction of colors can only be achieved with the best and most accurate color calibration and profiling. Rather than using the standard gamma of 2.2 or 1.8 as calibration target, ICS Remote Director uses a linear L* calibration gamma, mapping the display to a better match with the human visual system. F. Herbert, J. Kirkenaer and J. Ladson pointed out through psychophysical experiments performed to determine settings for accurate color reproduction on computer displays that by calibrating the display to linear L* rather than a gamma of 2.2, a significantly higher correlation was found comparing color patches in a viewing booth to the same colors presented on the computer display [5]. This experiment also demonstrated how important the viewing environment is, having a neutral background both on the display and for the hardcopy [6] with the proper amount of reference white shown in both cases.

Five (5) numeric criteria must be met in order for a system to be deemed to have passed certification and to be labeled as "SWOP Certified." [7]:

1. The difference between the characterization data set and the IT8/7.4 target is an average delta E94 $\leq$ 2.0 for all patches

2. The difference between the characterization data set and the IT8/7.4 target has a maximum delta E94 $\leq$ 6.0 for at least 95% of all patches.

3. Solid patches cyan, magenta, yellow, red green and blue on the IT/7.4 are delta E94 $\leq$ 6.0 from the characterization data set.

4. Differences between the characterization data set and patches on the IT8/7.4 target has white point of a delta L $\pm$ 2.0, a delta a $\pm$ 2.0 and a delta b $\pm$ 2.0 (excluding florescence).

Figure 1: Certification Results.

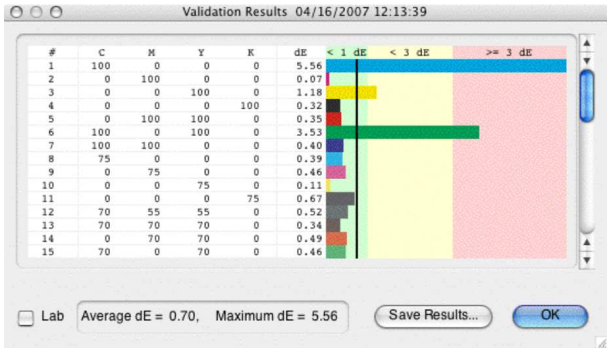

Figure 2: SWOP Validation Results.

5. Difference between the 50/40/40 gray balance target and the characterization data set has a delta E94 $\leq$ 2.0

These criteria were selected on the basis of measurements of monitor proofing systems currently certified. These criteria also draw parallels to hard copy specifications. It should be noted here that Cyan and sometimes green are problem colors for many displays and may in many cases be outside the gamut of the display. However, gamut mapping technology correctly applied brings the out of gamut color to the gamut boundary of the display in such a manner as to minimize any visual color difference.

In ICS Remote Director, for example, the results of calibrating the display and running through the certification process will yield the message shown in Figure 1.

Clicking on "Show Details" will give the display shown in Figure 2, showing each individual color of the IT8/7.4 target, and the actual delta-E for each color. Note that in this case, Cyan still passed with an error of 5.56. The other "problem colors" can be seen to be other solid colors, such as yellow and green, though well within specification limits.

If we were to compare the CMYK profile to the display profile, and map them in the same three-dimensional color space, you might get the result shown in Figure 3. Here the gamut for SWOP Coated Paper no. 3 is shown in the gamut of an older Apple Cinema Display, and in this case certification did not pass, as shown in Figure 4, though it failed on white point calibration, not solid colors as would be indicated in Figure 3, where the SWOP gamut exceeds the display gamut in the Cyans and Greens.

The technology developed for SWOP certification can easily be extrapolated to work for other printing standards or reference media, such as FOGRA or others. FOGRA has proposed three standard printing conditions, FOGRA30L, FOGRA39L and FOGRA40L. Characterization data for these conditions have been published and these can easily be used to generate reference CMYK profiles and included in the ICS Remote Director application as shown in the Figure 5, for selection and display certification.

Comparing the FOGRA30L profile to the Coated SWOP no. 3, the FOGRA profile gamut is significantly smaller and fits well within the SWOP gamut, as shown in Figure 6. Hence, certification using this FOGRA profile would pass if the system is already SWOP certified.

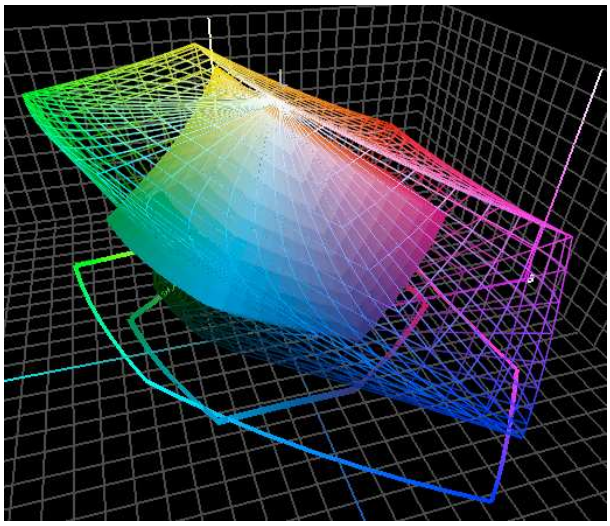

Figure 3: SWOP and Apple Cinema Display (Old).

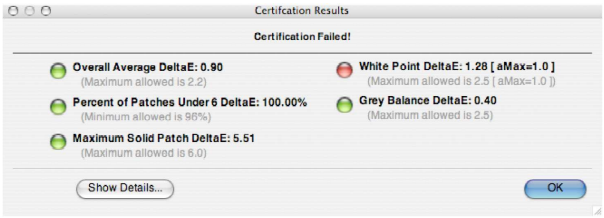

Figure 4: SWOP Certification on Apple Cinema Display (Old).

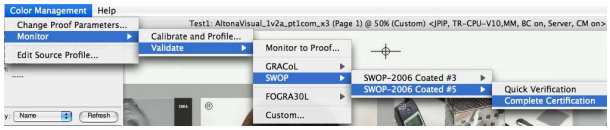

Figure 5: RD Pull-Down menu for Display Certification.

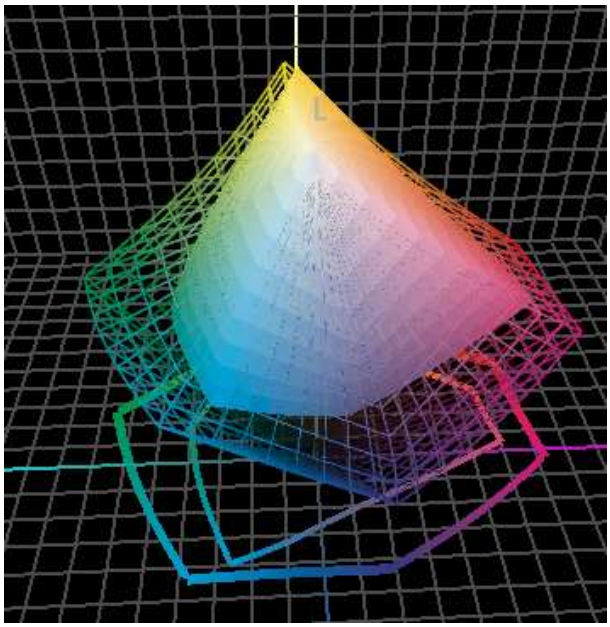

Figure 6: Comparison of SWOP and FOGRA Profiles

The profile itself is not perfect, and CMYK data transformed through the A2B1 table will not always yield the perfect response that actually generated the profile, that is comparing the same L*a*b* values as in the characterization data. We can run target CMYK values through the A2B1 tag, and compare the calculated L*a*b* value to the measured L*a*b* in the characterization set. For the FOGRA30L dataset we get errors of

$$\text{avg dE} = 0.36, \text{ max dE} = 0.71, \text{ stdev dE} = 0.09$$

which are actually very good results, hence display measurements should be very reliable.

It should also be noted that for SWOP or for FOGRA there are multiple printing conditions such as different paper types that all have to pass the certification process for the monitor proofing system to pass the complete certification process.

Conclusions

We have shown that through proper calibration and characterization of the display, and with a good source profile for soft proofing, accurate colors for the printing condition can be presented on the display. Measurements of these colors can be used to certify the display, and this certification process can be expanded to other standard or reference printing conditions.

References

[1] Gary G. Field: "Color Approval in the Graphic Arts", The Fifth Color Imaging Conference: Color Science, 1997.

[2] Ricardo J. Motta: "Computer Color Reproduction", SPIE, Vol 2414 p.2 (1996).

[3] IPA Color Proofing RoundUP Results – 2005, Dr. Abhay Sharma, Ed. (2005).

[4] IPA Color Proofing RoundUP Results – 2006, Dr. Abhay Sharma, Ed (2006).

[5] F. Herbert, J. Kirkenaer & J. Ladson: "Absolute and relative colorimetric evaluation for precise color on screen", Color Imaging VIII: Processing, Hardcopy, and Applications, pp 294-305.

[6] ISO/DIS 12646 "Graphic technology – Displays for colour proofing – Characteristics and viewing conditions." Section 4.7, p4.

[7] Dr. Chris Edge, Kodak, communication to the SWOP Committee, November 2006.

Additivity Based LC Display Color Characterization

Jean-Baptiste Thomas and Jon Yngve Hardeberg
ColorLab, Gjøvik University College (Norway)

Irène Foucherot and Pierre Gouton
Le2i, University of Burgundy (France)

Abstract

We introduce an additivity based method to perform color characterization of LC display devices. We focus here on the forward transform from the device RGB color space to XYZ tristimulus values. Chromaticity constancy is an assumption in all chromaticity matrix based characterization models, but in practice this assumption does not hold perfectly. The main contribution of this work is to define a model where the chromaticity non-constancy is not a source of error. Our method outperforms traditional approaches such as the PLCC and GOG models without needed more measurements than those. The proposed approach could be particularly useful for multi-display systems characterization as it is not time consuming and gives precise enough results.

Keywords: LCD, Color characterization, Projection displays.

Introduction

Characterization of color display devices is an important part of a color management system. The characterization of such a device defines the relationship between the device-dependent color space, typically RGB, and a device-independent color space describing the perceived color, typically XYZ which describes the color perception of the CIE standard observer. The forward transform make us able to predict the color which will be displayed (XYZ) for a given set of digital values input to the device (RGB) and the inverse (backward) transform will give us the digital values to input in order to display the desired color. Our work focuses on finding a forward model which is not subject to chromaticity non-constancy.

There exist a lot of methods to characterize color in a display device. Most part of them can be found in the following articles [1, 2, 3]. We could make the distinction between two main groups. The one which are performing 3D interpolation needs a lot of measurement and are computationally complex. However, they don't suppose any special device properties, i.e. the device can be consider as a black box, and no physical rules are assumed. It could be useful for example when you don't have any/enough information about the technology used. The models in the other group are trying to establish a mathematical model of the response of the device. For example, linearizing the intensity response curve of the display, by a global function or by interpolation, before applying a 3x3 chromaticity matrix to get the XYZ coordinates. This group of models do not need a lot of measurements but are making the assumption that the channels are independent and that the chromaticity of the primaries are constant. For instance, the response curve could either be a gamma shaped curve (defined by an offset and a gain) or a S shaped curve which could be defined by 4 parameters as in the S-Curve model [2].

In the case of a multi-display system or in the case of a projection device, we need an accurate characterization model which doesn't need a lot of measurement, as we could have to perform it on several displays or at several positions of the same display to correct for spatial non-uniformity [4]. Therefore the 3D LUT methods would be too heavy to be used in such a case, in spite of a good precision [1]. As desktop projectors are seldom belonging to CRT technology, the GOG model would not give good enough results. We would expect the classic PLCC [3] to give a good compromise between number of measurements, celerity and precision. A source of error in such a model is the non-chromaticity constancy of primaries (see fig.1.b and 2.b). One cause of this

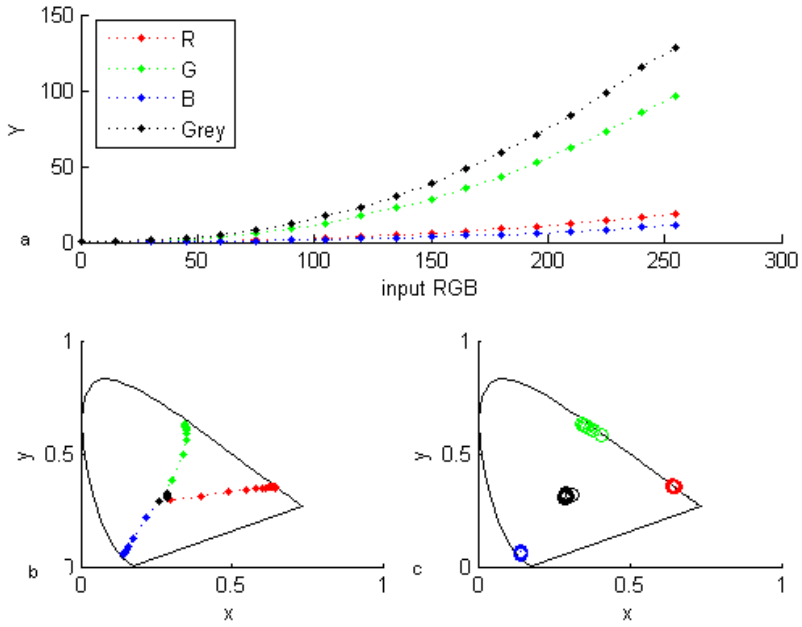

Figure 1: Projector 1. a : response curve for each channel and gray. b : chromaticity shift in xy diagram without black correction. c : Black corrected chromaticities.

is the influence of the 'chromaticity' of the black offset which is mixed with the color, and have more and more influence as the intensity decrease, i.e. the smaller the input value is, the more the chromaticity is attracted by the black. One way to overcome this problem is to remove this black offset before to perform the linearization and apply the matrix. It's working well in the case illustrated in fig.2.b and 2.c where the chromaticity shift keep almost on a line in the direction of the black, i.e. the black level is almost the only cause of chromaticity shift. The PLCC model then give correct results (see table 1). In other cases we can observe that this chromaticity shift is taking the shape of a coma, i.e. the main part of the chromaticity non-constancy is not only due to the black level, the technology itself play an important role (see fig.3.b and 3.c). An explanation is given by Marcu in [5], the LC component properties change with the intensity, so the spectra is modified with the intensity. Typically, in Marcu's experiment, for the (0, 0, 0) RGB input, the black is bluish because of the poor filtering power in the low wavelength. In such a situation, the black correction is not at all efficient and the model give poor results (table 1).

The main idea of our work is to make this shift not a problem, supposing a perfect additivity and channel independancy. Doing that, the error of the model will come only from the channel's non-independancy, and from the time and spatial non-uniformities. Obviously the interpolation method used will have some influence as long as we want to limit the number of measurements. In the following sections we present our approach and some results. Our conclusion gives a way to perform the inverse model.

Model

The method itself is quiet simple as long as the additive mixture of color is the base of so-called additive displays (as LC panels and projection devices). From the measurement of the XYZ coordinates of a sampling of the digital ramp of each channel (i.e. N values regularly spaced on the 256 possibilities for an 8 bits device), we will suppose the perfect additivity of the device. Moreover, we keep on considering channels as independants. Note also that we perform the black correction in the manner of PLCC.

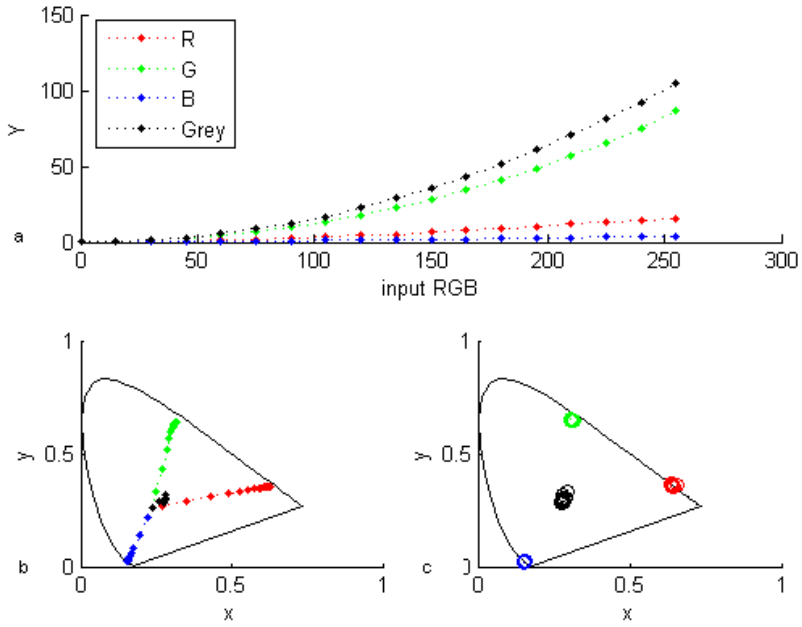

Figure 2: Projector 2. a : response curve for each channel and gray. b : chromaticity shift in xy diagram without black correction. c : Black corrected chromaticities.

Then a color XYZ_o output from a RGB_i input to the device would be expressed as

$$X_o = Xr_i + Xg_i + Xb_i$$

$$Y_o = Yr_i + Yg_i + Yb_i$$

$$Z_o = Zr_i + Zg_i + Zb_i$$

Where Nn_i is the value of the color from the channel n along the dimension of N for an input $_i$.

To generalize from the measurements to all the color space, we perform a 1D interpolation along each channel R, G, B for each color component X, Y, Z (i.e. 3×3 1D interpolations). Linear interpolation gives good results (see next section), and is already well implemented on a classical color management system. Therefore it would be easy to use this model with existing system and shift from a chromaticities matrix based model as PLCC to our approach without loosing any time as the matrix computation is replaced by linear interpolation.

Results

We have tested this forward model on 2 LCD projectors, the Panasonic PT-AX100E refered as projector 1, the 3M-X50, refered as projector 2. And on one LCD desktop panel, refered as monitor. We have compared the results with classic PLCC, and GOG characterization models. The interpolation method used were linear, cubic or spline performed with matLab. These results are based on a 18 patches by ramp measurements, for each device (see fig.1-3.a). We have calculated the ΔE^*_{ab} for the forward model from a set of 100 random RGB patches, the mean, the max and the standard deviation of these errors for each method are given in table 1.

We can obviously see that the PLCC without correction for black level gives so bad results. Correcting for black level, results are better. As we have said in the introduction, if the black correction is the main part of channel non-constancy, results are good. It is the case for projector 2 with a mean error of 1.78. In the other case, result are not efficient at all with 3.93. It's quiet strange to note that the PLCC with or without black correction give almost the same accuracy for the monitor.

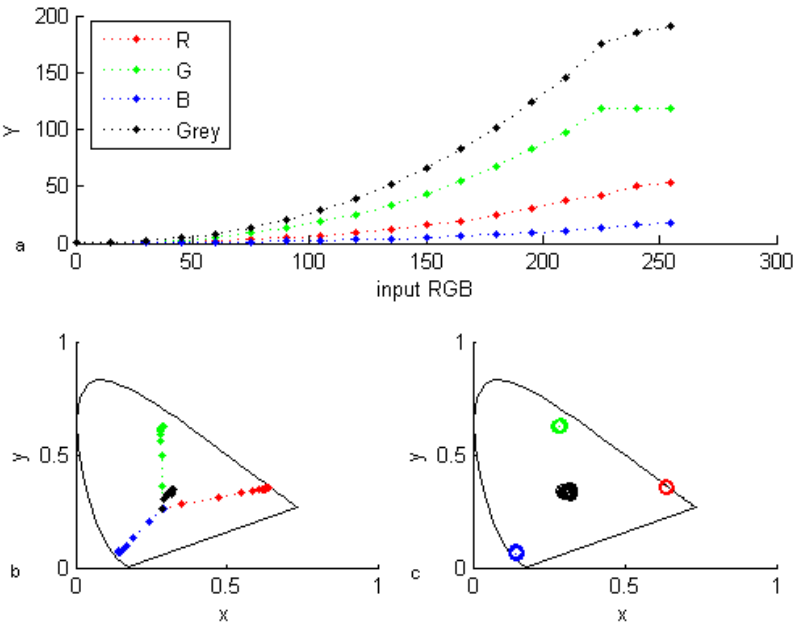

Figure 3: Monitor. a : response curve for each channel and gray. b : chromaticity shift in xy diagram without black correction. c : Black corrected chromaticities.

Mean, Max and standard deviation of ΔEa*b* for 100 random patches	PLCC	PLCC (black corrected)	GOG	Additive model (Linear interpolation)	Additive model (Cubic interpolation)	Additive model (Spline interpolation)
Projection 1	Mean : 6.42	3.93	3.96	1.41	1.35	1.32
	Max : 19.06	8.28	14.61	3.56	3.21	2.94
	Stddev : 4.28	2.15	2.62	0.63	0.53	0.5
Projection 2	Mean : 15.19	1.78	2.86	0.54	0.53	0.53
	Max : 55.62	2.96	11.41	1.64	1.54	1.61
	Stddev : 14.94	0.51	2.3	0.28	0.27	0.27
Monitor	Mean : 4.66	4.88	6.89	2.04	2.21	2.16
	Max : 12.08	9.36	45.54	4.55	5.20	5.36
	Stddev : 2.3	2.16	6.09	0.91	0.95	0.95

Table 1: Results

Projection 1	X	Y	Z
White (full intensity)	115	128.6	155.4
R+G+B (full intensity)	111.93	125.12	154.11
Difference (%)	2.67	2.71	0.83

Projection 2	X	Y	Z
White (full intensity)	93.97	105	135
R+G+B (full intensity)	94.81	103.96	136.9
Difference (%)	0.89	0.91	1.41

Monitor	X	Y	Z
White (full intensity)	188.1	191.1	209.9
R+G+B (full intensity)	187.59	190.53	210.91
Difference (%)	0.27	0.30	0.48

Table 2: Additive properties of tested displays.

As expected, the GOG model doesn't give so good results for these devices with a mean error of 3.96 and 2.86 respectively for projector 1 and 2, and with a mean error of 6.89 for the panel. Note that the settings of the monitor could be better adjusted to avoid the fact that the green channel saturate, doing that the GOG would give quiet better results. But seeing that our method give good result in such a case prove the robustness of the model.

With a linear interpolation, our additive model gives respectively 1.41, 0.54 and 2.04. We have reduced the mean error of the PLCC almost by 3 in the worst case. With other interpolation techniques results are quiet similar. The best results were obtained with Spline interpolation for projection device which gives mean error of 1.32 and 1.53, and with linear interpolation for monitor.

Maximum errors are quiet small too, around 1.6 for the projector 2, 3.2 for projector 1 and 5 for monitor.

Seeing at these results, we can see that our model overcome the classic PLCC and the GOG model for the forward transform. We can notice as well that the influence of the interpolation method is limited by the number of measurements on the ramp. With a smaller number of measurements, the interpolation would have more influence on the results.

We can notice as well that the additivity properties of tested displays is, as expected, still a source of errors. In Table 2 you can see the difference of additive quality of both projection displays. We have presented these results as in [2]. We can see, coupling information from table 1 and 2 that our results are poor as the device's quality for additivity decrease. However, the additivity quality of the monitor (table 2) is shown really good, but results are not as good as with projection devices. That mean that the channel interaction is big in this device.

Conclusion

We have defined a forward model for display characterization which is easy to implement as the PLCC, with noticeable better results. This model would be usefull to characterize multi-display systems and projectors, as it is easy to perform and doesn't need a lot of measurements.

The inverse model would be a bit more complex as there is no analytical solution. It could be performed by an optimization method to design a regular grid in XYZ, using the forward model. Then it's pretty easy to find an efficient algorithm to interpolate from this 3D LUT. Note that no more measurements would be needed to develop the inverse model, so it's possible to overcome one drawback of 3D LUT model.

Moreover, this model would be of great interest for multi-primaries displays or spectral approaches. This could be a part of our future works.

References

[1] Behnam Bastani, Bill Cressman, Brian Funt. "Calibrated color mapping between LCD and CRT displays: A case study". Color Research & Application, Volume 30, Issue 6, Pages: 438-447, 2005.

[2] Kwak Y, MacDonald L. "Characterization of a desktop LCD projector". Displays, Volume 21, Pages: 179-194, 2000.

[3] Post DL, Calhoun CS. "An evaluation of methods for producing desired colors on CRT monitors". Color research & Application, 14:172-186, 1989.

[4] Jon Y. Hardeberg, Lars Seime, and Trond Skogstad. "Colorimetric characterization of projection displays using a digital colorimetric camera", Proc. SPIE Int. Soc. Opt. Eng. 5002, 51, 2003.

[5] Marcu, G. et al., "Color characterization issues for TFTLCD displays", Proc. SPIE, Color Imaging : Device-Independent Color, Color Hardcopy, and Applications VII, Eschbach, R. and Marcu, G., Eds., Vol. 4663, 2002, 187-198.

Biography

Jean-Baptiste Thomas has received his bachelor's degree in Physics and applications in 2004 and his master's degree in Image, Vision and Signal in 2006 from the University Jean Monnet, France. He is currently pursuing the PhD degree at the University of Burgundy, France. His research focuses on colors in projection and tiled projection displays.

Color Mixing and Color Separation of Pigments with Concentration Prediction

Pesal Koirala, Markku Hauta-Kasari, Birgitta Martinkauppi, and Jouni Hiltunen
Department of Computer Science and Statistics, University of Joensuu, Finland.
{pkoirala,mhk,jbm,jouni.hiltunen}@cs.joensuu.fi

Abstract

In this study, we propose a color mixing and color separation method for the pigments painted on plastic surface based on Kubelka-Munk (KM) model. Eleven different pigments with seven different concentrations have been used as training set.The amount of concentration of each pigment in the mixture is estimated from the training set by using the least-square pseudo-inverse calculation. The result depends on the number and type of pigments selected for calculation. At most we can select all pigments. The combinations resulted with negative concentrations or unusual high concentrations are discarded from the list of candidate combination. The optimal pigment's set and its concentrations are estimated by minimizing the reflectance difference of given reflectance and predicted reflectance.

Keywords: Color prediction, Kubelka-Munk method, Saunderson correction, Reflectance, Least-square pseudo-inverse calculation.

1. Introduction

Originally KM theory is a model of the light travelling in two directions in the materials [9]. The basic KM theory is admissible to the diffuse illumination of particular coating. The KM theory is of great importance in many areas of applied research and has been used for the optical properties of decorative and protective coatings, paints, paper, pigmented polymers, fibers and wool, thermal insulation, biological systems, and in medical physics [12]. KM method assumes a linear relationship between scattering coefficient S and the absorption coefficient K, and this makes the computation process faster. Further improvement in this method was achieved by Saunderson correction [7]. Saunderson correction converts the total reflection to the body reflection on which the KM theory works. The revised KM theory [8] has been used for ink, paper and dyed paper. Monte Carlo simulations, Expert systems or Neural networks and Mie theory have been immerged as the alternative as well as collaborative method of KM model. Independent component analysis (ICA) [2] may be used as the reflectance separation but further research is required.

In this study, we have implemented single constant KM theory for the pigments located on the plastic. Our method predicts the reflectance of mixture from the given set of pigments with different concentration. In additions our method is capable of predicting the accurate concentrations and reflectance of mixed pigments from the given reflectance of mixture. This color separation method also uses the color mixing method as a sub-problem since the given mixture is compared with predicted reflectance of mixture to minimize the reflectance difference. There are different methods for evaluating these differences. CIE color difference equations (CIE Lab, CIE LUV CIE94 etc), Spectral curve difference metrics (Root mean square error (RMS), Goodness of Fit Coefficient (GFC)), Metamerism indices and Weighted rms metrics [5] can be used to calculate color differences during minimizing reflectance process. In proposed method CIE LAB error, Goodness of Fit Coefficient (GFC) and Mean square error (MSE) were computed to calculate quantitative value of reflectance matching.

The reflectance of training sets and test sets were measured by spectrometer called AvaMouse [1] with $45^o/0^o$ geometry under circular illumination. In total eleven different samples were used as training sets. Seven different concentrations of each sample were prepared.

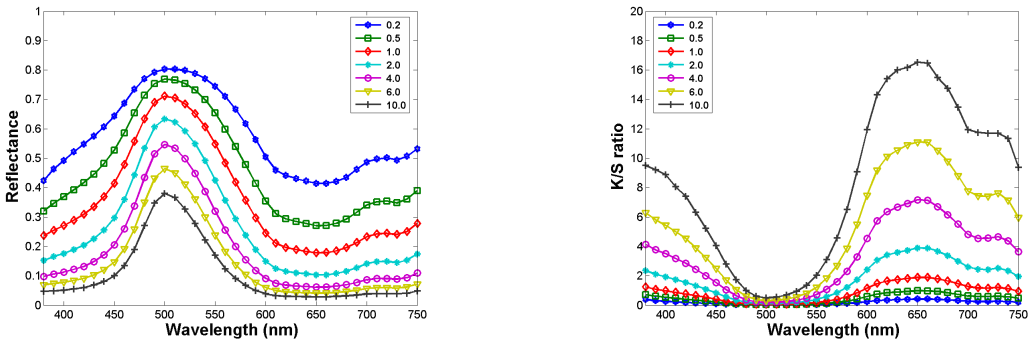

Figure 1: Reflectance and K/S ratio of a sample pigment at different concentrations [0.2 0.5 1 2 4 6 10] gram in one litre of filling material.

2. Kubelka-Munk Theory

The key assumption in applying the KM theory is that the light within the pigment layer is completely diffuse and there can not be changed in refractive index in the samples boundaries [11]. The specular component is excluded by geometry measurement. Many modern spectrometers are capable to measure reflectance factor without changing the refractive index in the samples boundaries [4]. However if the available spectrometer can measure only total reflectance, the measured reflectance should be corrected before applying to KM model by Saunderson correction [7] as shown in Eq.(1).

$$R_\lambda = \frac{r_\lambda - K_1}{1 - K_1 - K_2(1 - r_\lambda)} \tag{1}$$

Where, r_λ is the total reflectance which should be normalized between [0, 1] in each wavelength λ, K_1 is the Fresnel reflection coefficient for the collimated light and K_2 is the Fresenel reflection coefficient for diffuse light striking the surface from inside. The value of K_1 is 0.04 for plastic material since plastic has the refractive index of 1.5 [11]. The value of K_2 usually lies between 0.4 and 0.6 [7]. The optimized value of K_2 should be calculated practically.
Once the internal reflectance is calculated by the KM mixing law, the total reflectance is computed by reversing Eq.(1) as:

$$r_\lambda = K_1 + \frac{(1 - K_1)(1 - K_2)R_\lambda}{1 - K_2 R_\lambda} \tag{2}$$

For complete hiding [3], opaque materials [11]; the internal reflectance was estimated by KM model using the ratio of absorption coefficient K_λ and scattering coefficient S_λ.

$$R_\lambda = 1 + \left(\frac{K}{S}\right)_\lambda - \sqrt{\left(\frac{K}{S}\right)_\lambda^2 + 2\left(\frac{K}{S}\right)_\lambda} \tag{3}$$

The widely used K over S ratio is obtained reversing Eq.(3):

$$\left(\frac{K}{S}\right)_\lambda = \frac{(1 - R_\lambda)^2}{2R_\lambda} \tag{4}$$

Figure 1 illustrates the measured internal reflectance factor and its conversion to K over S value from Eq.(4) for the known concentration of [0.2 0.5 1 2 4 6 10] gram in one liter filling material. The scattering and absorption coefficients of mixture are described as the linear combination of scattering and absorption coefficients of mixed pigment scaled by the concentration of the

pigments as shown in Eq.(5). This method is well known as two constant KM model.

$$\left(\frac{K}{S}\right)_{\lambda,mix} = \frac{\sum_{i=1}^{n} C_i K_{\lambda,i}}{\sum_{i=1}^{n} C_i S_{\lambda,i}} \tag{5}$$

The individual absorption and scattering coefficients required for Eq.(5) are calculated by using the white set (setting scattering 1 in every wavelengths), masstone (100 % relative percentage pigment) and tint (pigment mixed with white) [6]. In the case, the substrate has more scattering properties than the coated pigment the Eq.(5) is reduced to more simple form called the single constant KM model see Eq.(6). The ratio of K/S is used instead of calculating individual K and S. In this paper we have used single constant KM model.

$$\left(\frac{K}{S}\right)_{\lambda,mix} = \sum_{i=1}^{n} C_i \left(\frac{k}{s}\right)_{\lambda,i} \tag{6}$$

Where,

$\left(\frac{K}{S}\right)_{\lambda,mix}$	ratio of absorption and scattering of pigment mixture.
n	number of pigments in mixture.
C_i	concentration of i^{th} pigment in mixture by weight of dry pigment.
$\left(\frac{k}{s}\right)_{\lambda,i}$	ratio of absorption and scattering of i^{th} pigment for unit concentration.

3. Color Mixing

Given a set of pigments with reflectance curve, we can get the reflectance curve for any specified mixture of pigments by using Eqs.(3), (4) and (6). If the available spectrometer can measure only the total reflectance, then Saunderson correction is also considered (see Eqs.(1) and (2)). In our experiment we have measured the reflectance by AvaMouse handheld reflection spectrometer with annular measuring geometry with in range of 380 to 750 nm. The AvaMouse measures touching coated surface and distance between camera and surface are shorter in comparison to spectrophotometer measurement. So the measured reflectance is equal to body reflectance, as a result Saunderson correction is not applied to the measurement by AvaMouse.
The unit k/s of each pigment is required to predict the specified mixture of pigments from the set of pigments in training set with specified concentration. The Eq.(7) gives the method to calculate unit k/s value of single colorant since the colorant is mixed with white pigments.

$$\left(\frac{k}{s}\right)_{\lambda,1} = \frac{\left(\frac{K}{S}\right)_{\lambda,mix} - C_W \left(\frac{k}{s}\right)_{\lambda,w}}{C_1} \tag{7}$$

Where,

C_1	concentration of pigments.
C_W	concentration of white pigments used as substrate.

Each colorant in the training set has seven different concentrations (see Figure 1). From these seven different concentrations one representative unit k/s is calculated by using least-square pseudo-inverse calculation. Figure 2 illustrates the unit k/s ratio and its normalized spectrum in wavelength 650 nm. The normalized spectrums of unit k/s ratio of same pigment from different concentrations should be almost the same for proper selection of a sample set. Figure 3 illustrates the reflectance curves obtained by mixing three samples with the concentration of [0.5 0.7 3.0] gram. The color of reflectance of samples and mixture is visualized in monitors by calculating the tristimulus values X, Y and Z from reflectance and then converting them to device RGB coordinate system by using linear transformation [11] [10].

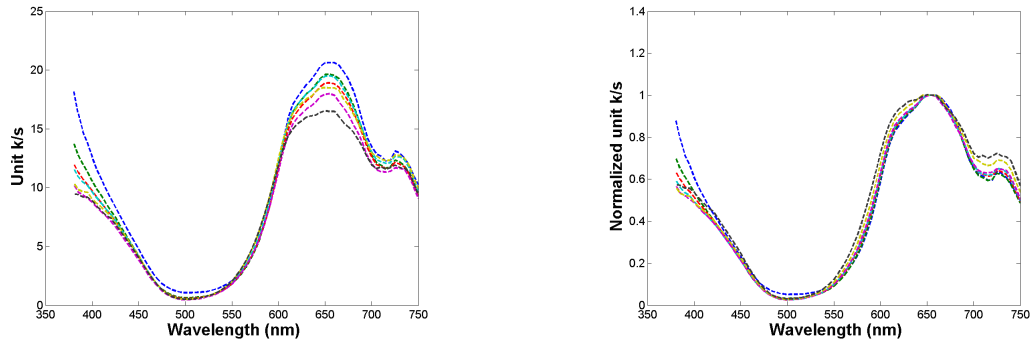

Figure 2: The unit k/s and normalized unit k/s at 650 nm wavelength calculated from the samples at different concentrations.

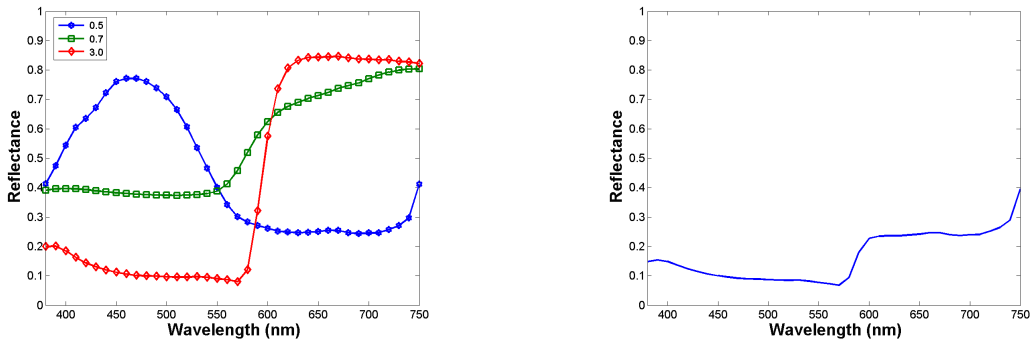

Figure 3: Three different colorants reconstructed with 0.5, 0.7 and 3.0 gram pigment concentration. The right image is the resultant reflectance computed mixing these three pigments.

4. Color Separation and Concentration Prediction

The concentration of the pigments can be estimated from Eq.(10) if the K/S value of mixture and the unit k/s value of mixed pigments are known. The number of concentrations in mixture is equal to number of pigments (n) mixed and that should be less than the number of wavelengths sampled to present the reflectance curve. So only the n number of wavelengths can be selected to solve the n number of concentrations [11]. However choosing n number of different wavelengths results the different concentrations, so for more stable result least-square pseudo-inverse calculation is used to calculate concentration considering all visible range wavelengths (see Eqs.(8)-(10)). Similarly the unit k/s value of each pigments used in the mixture can be calculated by least-square pseudo-inverse methods if K/S value of the mixture and the concentration of pigments used in mixture are known (see Eq.(12)). After knowing the concentration and unit k/s value, the reflectance of the pigments is predicted by using Eqs.(6) and (3) consecutively. The Eq.(6) is represented in matrix form in Eq.(8) extending for all wavelengths.

$$\begin{bmatrix} \left(\frac{K}{S}\right)_{380,mix} - \left(\frac{k}{s}\right)_{380,W} \\ \vdots \\ \vdots \\ \vdots \\ \left(\frac{K}{S}\right)_{750,mix} - \left(\frac{k}{s}\right)_{750,W} \end{bmatrix} = \begin{bmatrix} \left(\frac{k}{s}\right)_{380,1} & \cdots & \cdots & \left(\frac{k}{s}\right)_{380,n} \\ \vdots & \vdots & \vdots & \vdots \\ \vdots & \vdots & \vdots & \vdots \\ \vdots & \vdots & \vdots & \vdots \\ \left(\frac{k}{s}\right)_{750,1} & \cdots & \cdots & \left(\frac{k}{s}\right)_{750,n} \end{bmatrix} \begin{bmatrix} c_1 \\ \vdots \\ \vdots \\ c_n \end{bmatrix} \tag{8}$$

Where,

$$C = \begin{bmatrix} c_1 \\ : \\ : \\ c_n \end{bmatrix} X = \begin{bmatrix} \left(\frac{k}{s}\right)_{380,1} & \cdot\cdot & \cdot\cdot & \left(\frac{k}{s}\right)_{380,n} \\ : & : & : & : \\ : & : & : & : \\ : & : & : & : \\ \left(\frac{k}{s}\right)_{750,1} & \cdot\cdot & \cdot\cdot & \left(\frac{k}{s}\right)_{750,n} \end{bmatrix} Y = \begin{bmatrix} \left(\frac{K}{S}\right)_{380,mix} - \left(\frac{k}{s}\right)_{380,W} \\ : \\ : \\ : \\ \left(\frac{K}{S}\right)_{750,mix} - \left(\frac{k}{s}\right)_{750,W} \end{bmatrix}$$

Eq.(8) is represented as:

$$Y = XC \tag{9}$$

The least-square pseudo-inverse calculation (see Eq.(10)) is used to find the concentration of pigment. The number of pigments mixed (n) should be less than number of wavelengths. So alternatively by choosing the n number of different wavelengths, the problem can be solved. Nevertheless the entire wavelength calculation gives more robust result.

$$C = \left(\bar{X}X\right)^{-1} \bar{X}Y \tag{10}$$

Deriving $\bar{X}$ from Eq.(9)

$$\bar{X} = \left(C\bar{C}\right)^{1} C\bar{Y} \tag{11}$$

Considering a more complex case where we have only been given the reflectance of mixture and our task is to estimate the concentration and the reflectance of the pigments used in the mixture. The problem is solved by using the unit k/s values of each pigment of the training set. The predicted concentrations and used unit k/s of each iteration are employed to estimate the reflectance (see Eq.(6) and (3)). This process is repeated for all possible combinations. Eq.(12) shows the total number of combinations to be computed.

$$\begin{pmatrix} N \\ n \end{pmatrix} = \frac{N!}{(N-n)!n!} \tag{12}$$

Where,

N	number of pigments in training sets.
n	number of pigments used in mixture.

The unit k/s and predicted concentrations are chosen so that estimated reflectance using this concentration and unit k/s has minimum differences with given reflectance of mixture. The differences of the reflectance are calculated by using color difference of Lab color spaces [11] [10], Goodness of fit coefficients and Mean square error [5]. The Computation step predicting optimal concentrations used in the mixture is shown below.

---

1. Compute unit k/s ratio of each training set.
2. Convert reflectance of test set R_{mix} to K/S ratio using Eq.(4).
3. Choose n number of pigments in mixture.

   Repeat step 4 to 8 for all combination $\begin{pmatrix} N \\ n \end{pmatrix}$.
4. Predict concentrations using Eq.(10) and store row wise in matrix *concentration*.
5. The negative concentrations and unexpected high concentrations are neglected.

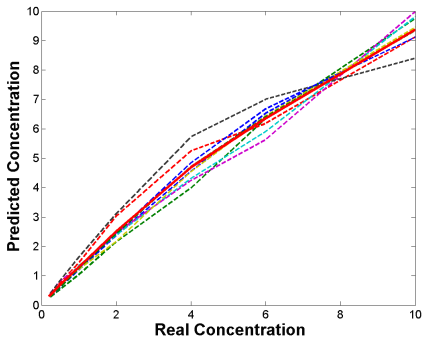

Figure 4: Real concentration verses predicted concentration. Concentration is represented in gram. The dotted line shows for the pigments and solid line is the average of all dotted lines.

6. Predict $(K/S)_P$ ratio of mixture using predicted concentrations and unit k/s ratio from training set, see Eq.(6) or Eq.(8).

7. Determine reflectance R_P using $(K/S)_P$, see Eq.(3).

8. Calculate difference ΔE between R_{mix} , and R_P and store ΔE in array *error*.

9. Order the matrix concentration according to array error sorted in ascending order for Lab difference and MSE, and descending order for GFC.

The real concentration of pigments used in mixture and corresponding predicted concentrations by our method is illustrated in Figure 4. The predicted concentrations of colorants can be corrected by fitting the predicted concentration with real concentration by using interpolation methods. However, in advance we should have the relation between real concentration and predicted concentrations of each pigments of the training set.

5. Conclusion

The basic theory of KM method was discussed. The method to predict the reflectance of mixture made from the pigments with arbitrary concentration was described. Computation process for the concentration prediction and separated color prediction was described. Our future work will consider more accurate color separation and concentration prediction from the given transparent and translucent object by KM methods and revised KM methods [8] and independent component analysis [2].

References

[1] http://www.avantes.com/news/avamouse.pdf 3-3-2007.

[2] Hyvärinen A., Karhunen J., and Oja E. *Independent Component Analysis*. John Wiley and Sons, 2001.

[3] Haase C.S. and Meyer G.W. Modelling pigmented materials for realistic image synthesis. *ACM Transactions on Graphics*, 11(4):305–335, October 1992.

[4] Bondioli F., Manfredini T., and Romagnoli M. Color matching algorithms in ceramic tile production. *Journal of the European Ceramic Society*, 26:311–316, 2006.

[5] Francisco H., Mitchell R., and Berns R.S. Comparative study of metrics for spectral match quality. *First European Conference on Colour Graphics, Imaging, and Vision*, pages 492–496, 2002.

[6] Davinson H.R. and Hemmendinger H. Color prediction using the two-constant turbid-media theory. *Journal of the Optical Society of America*, 56(8):1102–1110, August 1966.

[7] Saunderson J.L. Calculation of the color pigmented plastics. *Journal of Optical Society of America*, 32:727–736, December 1941.

[8] Yang L. and Kruse B. Revised kubelka-munk theory. i. theory and application. *Journal of the Optical Society of America*, 21(10):1933–1940, October 2004.

[9] Kubelka P. New contributions to the optics of intensity ligh scattering materials. part i. *Journal of the Optical Society of America*, 38(5), May 1948.

[10] Kuehni R.G. *Color an Introduction to Practice and Principles.* John Wiley and Sons, USA, 1997.

[11] Berns R.S. *Principles of Color Technology.* John Wiley & Sons, New York, third edition, 2000.

[12] Vargas W.E. and Niklasson G.A. Applicability conditions of the kubelka-munk theory. *Applied Optics*, 36(22):5580–5586, August 1997.

Video-based analysis for facial skin appearance with automatic face tracking

Takao Makino, Koichi Takase, Norimichi Tsumura, Toshiya Nakaguchi, and Yoichi Miyake
Graduate School of Science and Technology
Chiba University, Yayoi-cho, Inage-ku, Chiba,263-8522, Japan

Introduction

The analysis and synthesis for facial skin appearance play an important role in the filed of cosmetology and entertainment. Figure 1 shows a skin analysis and synthesis system used in the filed of cosmetology. The current condition of skin texture is measured as a high resolution image in the lighting box. The measured image is analyzed by our skin color separation technique [1] into melanin, hemoglobin and shading components. The skin melanin texture is controlled to show the change of texture by aging. This system is used for the customer to show the necessity of applying the cosmetics. However, the appearance of skin also changes drastically by changing the distribution of illumination. The information from single image is not enough in analyzing the change of skin appearance under various illuminations.

In this paper, we propose a video-based analysis for the facial skin appearance under various illuminations with an automatic face tracking technique. To analyze the change of skin appearance under various illuminations, the face is illuminated from various positions of the light sources, and the changes of facial appearance are recorded as video stream during this measurement. The recorded video stream is analyzed to obtain BRDF at the point on the facial skin. However, since the subject is not still during the measurement, measurement errors are caused by the facial movement. The automatic facial tracking is necessary to compensate the facial movement to perform the accurate BRDF measurement on the arbitrary facial point. Since the conventional face tracking techniques [2, 3] can not be used for the face illuminated from various positions of the light sources, we build a new face tracking technique which is robust to the various shading on the face. The proposed tracking is the technique to track the facial movement and arbitrary points on the facial skin by using two facial features that are less influenced by the shading. Arbitrary points on the facial skin are tracked with their 3D coordinates and the estimated facial movement. By using this technique, BRDF of the arbitrary facial point can be measured from the video stream.

Video-based analysis for facial skin appearance

Figure 2 shows an overview of our video-based analysis for facial skin. The system consists of a video camera and a movable light source. The subject sits in front of the video camera without keeping his or her head still. Since the head of the subject is not kept still, the subject can feel relaxed during the measurement. The face is illuminated from various positions by rotating the light source around the subject. The changes of facial appearance are recorded as video stream. In the recoded video stream, the influence of the facial movement is compensated with the tracking for the facial movement and target facial points. The tracking result of the facial movement is used to estimate the directions of incident light and the video camera after the facial movement. The tracking results of target facial points are used to estimate the position of target facial points after the facial movement. The compensated video stream is analyzed to obtain discrete pixel values on measurement points under various illuminations. Continuous BRDF is calculated by fitting the BRDF model[4] to discrete pixel values, the direction of incident light and the direction to the video camera. The calculated BRDFs are used to reproduce the appearance of the skin under various illuminations.

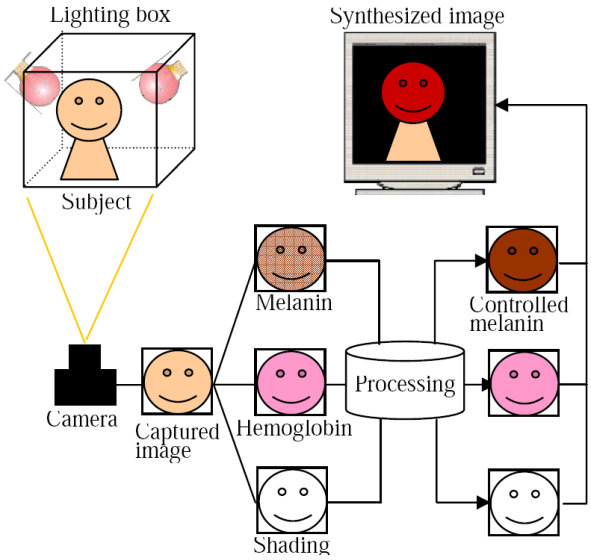

Figure 1: The conventional skin melanin texture control system.

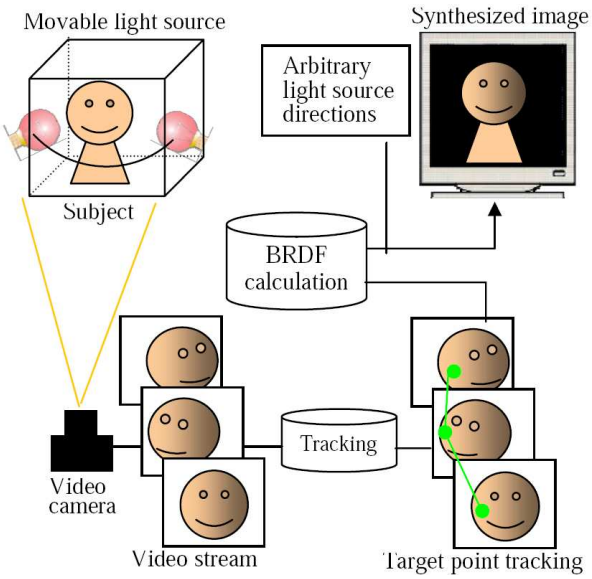

Figure 2: The overview of the proposed video-based analysis.

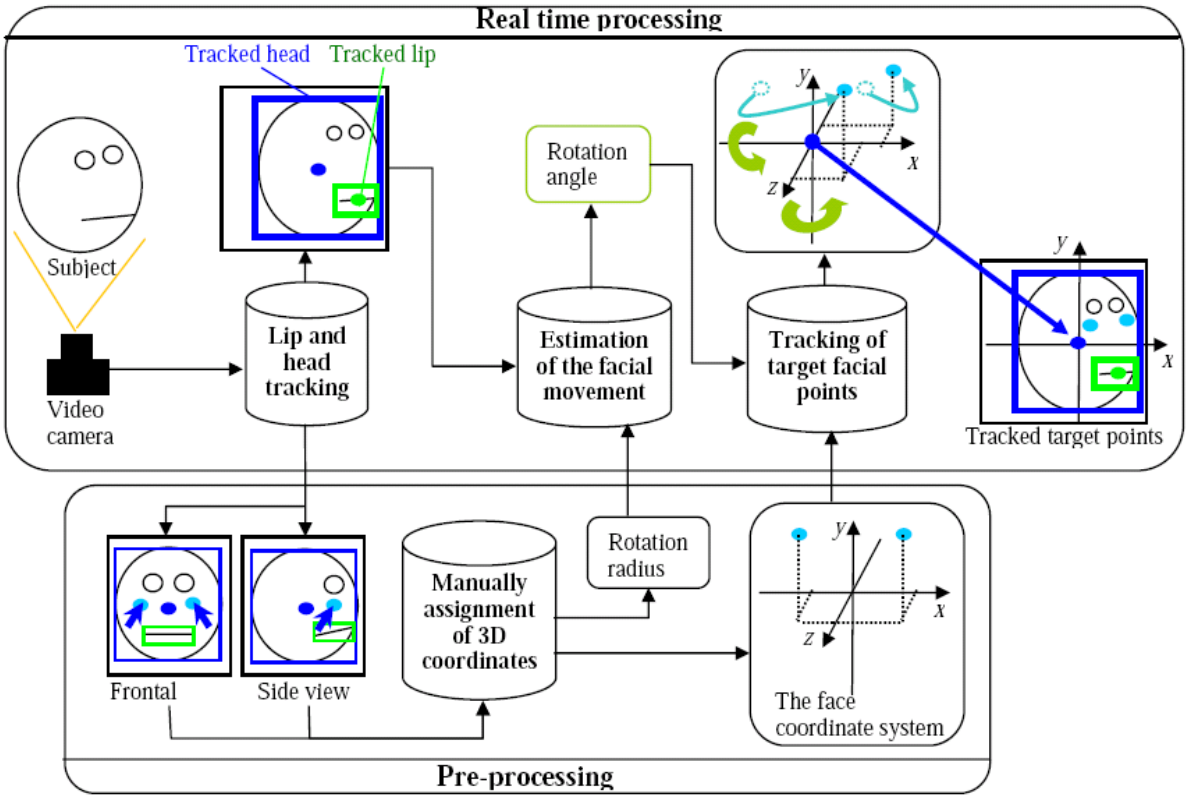

Figure 3: The flow of the proposed tracking technique.

Robust face tracking technique under various illuminations

We propose a robust technique for the shading to track the facial movement and arbitrary target points on the facial skin. This technique can track the parallel shift to x and y directions and the rotation around the x axis and y axis. Figure 3 shows the flow of the proposed tracking technique. In this flow, arbitrary target points are set at cheeks for the example in explanation. The technique consists of four components: 1) lip and head tracking, 2) the estimation of the facial movement, 3) the manually assignment of 3D coordinates, and 4) the tracking of target facial points.

1) Lip and head tracking

Coordinates of the lip (x_l, y_l) and the head center (x_h, y_h) are tracked on every frame of the video stream. Figure 4 shows the example of the tracking of the lip and the head center. A combining mean shift and Kalman filter [5] is used to track (x_l, y_l) and (x_h, y_h). This is the technique to track the arbitrary colored object in real-time. The coordinate of the lip (x_l, y_l) is tracked by the red color object. The head is tracked by the skin color and the hair color object, and its center (x_h, y_h) is used to the facial movement estimation. This head tracking is not affected by the shading. Therefore, this estimation can be used under any illuminations if the lip is captured in the image.

2) Estimation of the facial movement

In this processing, the parallel shift vector t and the rotation angles θ, and ϕ are estimated by using (x_l, y_l), (x_h, y_h), and the radius of the facial rotation. Figure 5 shows the overview of face rotation angles estimation. θ is the angle of the rotation around the y axis(azimuthal rotation),

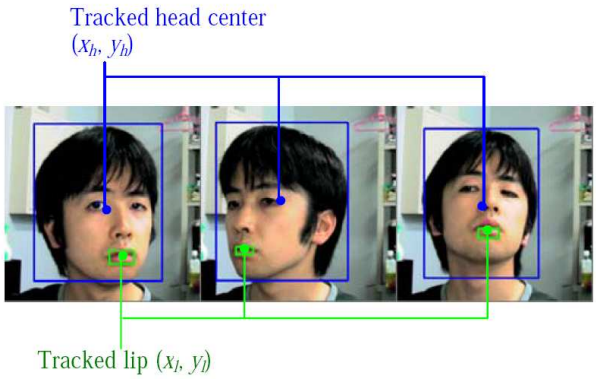

Figure 4: The example of the tracking of the lip and the head center.

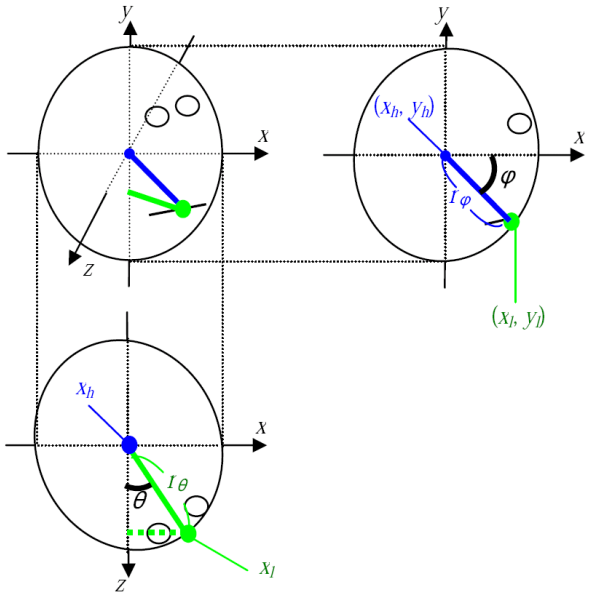

Figure 5: The overview of face rotation angles estimation.

and ϕ is the angle of the rotation around the x axis(elevation rotation). The radius of the facial rotation angle θ and ϕ is r_θ and r_ϕ respectively. We will describe how r_θ and r_ϕ are obtained later. In the proposed technique, the head center is assumed as an origin of the facial rotation. Therefore, θ and ϕ are estimated as

$$\theta = \sin^{-1}\left(\frac{x_l - x_h}{r_\theta}\right) \quad \phi = \sin^{-1}\left(\frac{y_l - y_h}{r_\phi}\right) \tag{1}$$

The parallel shift vector t is estimated as

$$t = [x_h - x_{y,1}, y_{h,1}]^T \tag{2}$$

where $(x_{h,1}, y_{h,1})$ is the coordinate of the head center in the first frame of the video stream

3) Manually assignment of 3D coordinates

The 3D coordinates of arbitrary target points and the radius of the facial rotation are obtained manually by using

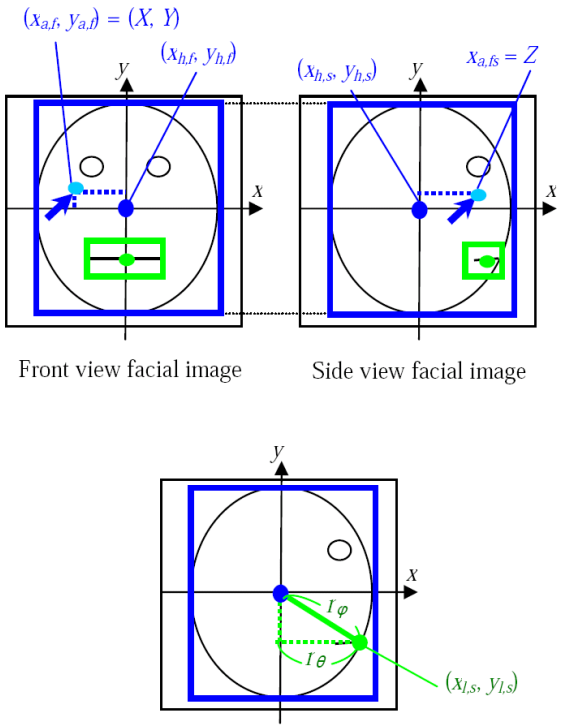

Figure 6: The assignment of 3D coordinate and the radius of the facial rotation.

front and side view facial images. Figure 6 shows the overview of obtaining the 3D coordinate (X, Y, Z) and the radius of the facial rotation r_θ and r_ϕ . (X, Y, Z) is obtained to assign the target position by the mouse click. It is obtained as

$$(X, Y, Z) = (x_{a,f} - x_{h,f}, y_{a,f} - y_{h,f}, x_{a,s} - x_{h,s}), \tag{3}$$

where $(x_{h,f}, y_{h,f})$, $(x_{h,s}, y_{h,s})$ is the coordinate of the tracked head center in the front and side view facial image respectively, and $(x_{a,f}, y_{a,f})$, $(x_{a,s}, y_{a,s})$ is the coordinate of the assigned point in the front and side view facial image respectively. Z is obtained to assign the target position in the side view facial image since x coordinate can be considered as z coordinate in the side view facial image. The matrix of 3D coordinates F is obtained by iterating this assignment for arbitrary times. It is shown as

$$F = \begin{pmatrix} X_1 & Y_1 & Z_1 \\ X_2 & Y_2 & Z_2 \\ & \vdots & \\ X_n & Y_n & Z_n \end{pmatrix}^T , \tag{4}$$

where (X_k, Y_k, Z_k), $(k = 1, 2, \ldots, n)$ is the k-th assigned 3D coordinate and n is the number of iteration. r_θ and r_phi are obtained as

$$r_\theta = x_{l,s} - x_{a,s}, \quad r_\phi = \sqrt{r_\theta^2 + (y_{l,s} - y_{a,s})^2}, \tag{5}$$

where $(x_{l,s}, y_{l,s})$ is the coordinate of the tracked lip in the side view facial image. These are used in Eq. (1).

4) Tracking of target facial points

Target points assigned in pre-processing are tracked by using F, θ, and ϕ. Figure 7 shows the overview of the tracking of target facial points. Each coordinate of F is represented as a 3D

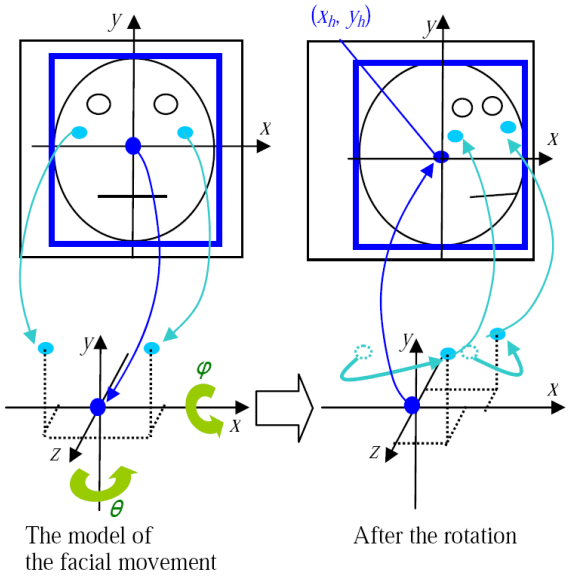

Figure 7: The model of the facial movement and target points tracking.

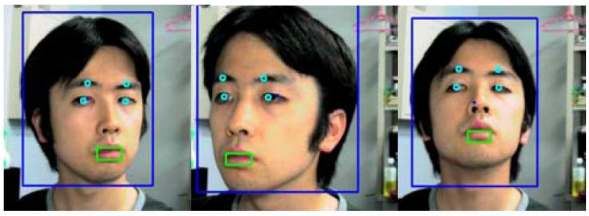

Figure 8: The result of eyes and eyebrows tracking.

point in the face coordinate system. The head center is the origin of this coordinate system. This coordinate system can rotate around the x axis and y axis. The target point tracking is performed to rotate 3D points by using θ and ϕ, and project to the image plane. The rotation matrix R which is used for the rotation is

$$R = \begin{pmatrix} \cos\theta & 0 & \sin\phi \\ 0 & \cos\phi & -\sin\theta \\ 0 & 0 & 1 \end{pmatrix}. \tag{6}$$

The matrix of tracked 3D coordinates F' is obtained as

$$F' = \begin{pmatrix} R & h \\ 0_3^T & 1 \end{pmatrix} F \tag{7}$$

$$0_3^T = (0\ 0\ 0)^T$$

$$h = \begin{pmatrix} x_h \\ y_h \\ 0 \end{pmatrix}.$$

The x and y coordinates of F' are the coordinates of the tracked point in the image plane. Figure 8 shows the result of eyes and eyebrows tracking. The green and blue rectangles show the lip and the head position respectively. Cyan circles show the results of eyes and eyebrows tracking. These points can be tracked in spite of various face movements.

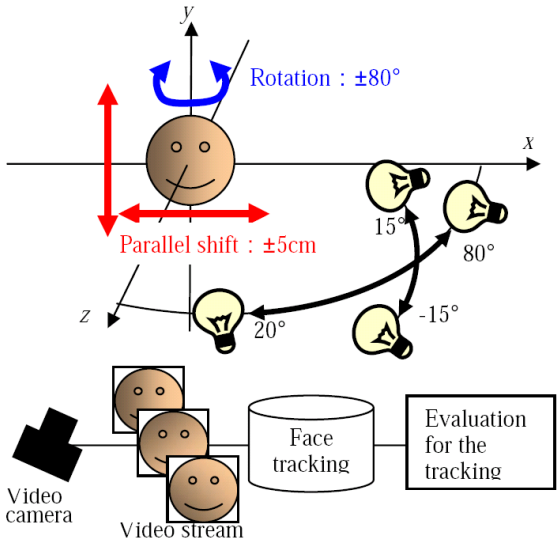

Figure 9: Geometry of the experiment.

Experimental evaluation for the proposed tracking technique

In this section, the effect of the proposed tracking technique is evaluated by the experiment. The geometry of this experiment is shown in Figure 9. A model of human face is used as the subject of this experiment since it is easy and accurate to obtain the actual movement. The face is illuminated by the light source with an azimuthal angle of 20°–80° and an elevation angle of −15°–15°. In each illumination angle, the face is moved ±5cm to horizontally(along the x axis) and vertically(along the y axis) and rotated with an azimuthal angle of −80°–80° around the center of the face model. These movements of the face under various illuminations are tracked and estimated with the proposed tracking technique.

Table 1 shows the estimation error of the parallel shift by the proposed tracking technique at three angles of the light source, and the average and maximum of the estimation error at all angles of the light source. These results show that the estimation error of the parallel shift is within 1cm under various illuminations.

Table 2 shows the estimation error of the rotation by the proposed tracking technique at four angles of the light source, and the average and maximum of the estimation error at all angles of the light source. The cell with dash indicates that the tracking failed in Table 2. The average of the estimation error is within 6°. The proposed technique fails to track the rotation of the face under illuminations that the lip is covered with the shading. However, the proposed technique can track the rotation angle of 0°–20° under the light source with an azimuthal angle of 80°. It is thought that the proposed technique has enough accuracy for the subject tracking in BRDF measurement system.

Experiment: Video-based BRDF measurement

In this section, we performed the experiment of the proposed video-based analysis technique. This experiment measures BRDF of four facial points on the moving subject.

Figure 10 shows the geometry of this experiment. The subject of this experiment is the model of human face. The face is illuminated by the light with an azimuthal angle of 0°–65° and an elevation angle of 15°. BRDF is measured at four facial points, forehead, cheek, lip and nose. In this experiment, BRDF is measured in three different conditions of the face movement. One is the condition that the face is kept still. Measured BRDF in this condition is the ground

Table 1: The estimation error of the parallel shift [cm].

	Direction and distance of the parallel shift			
Angle of the light source (azimuth, elevation)	Horizontally 5cm	Horizontally -5cm	Vertically 5cm	Vertically -5cm
(20°, 15°)	1.00	0.50	1.00	0.25
(60°, 15°)	0.10	0.73	0.30	0.70
(40°, -15°)	0.30	0.60	0.30	0.10
Average error at all illuminations	0.40	0.46	0.47	0.23
Maximum error at all illuminations	1.00	0.73	1.00	0.70

Table 2: The estimation error of the rotating [degree].

	Angle of the rotation			
Angle of the light source (azimuth, elevation)	**20°**	**40°**	**60°**	**80°**
(20°, 15°)	**0.50**	**1.80**	**6.30**	**5.30**
(40°, -15°)	**1.30**	**2.20**	**2.00**	–
(60°, 15°)	**3.00**	**6.00**	–	–
(80°, 15°)	**2.30**	–	–	–
Average error at all illuminations	**1.43**	**2.90**	**5.10**	**5.30**
Maximum error at all illuminations	**3.00**	**6.00**	**7.00**	**5.30**

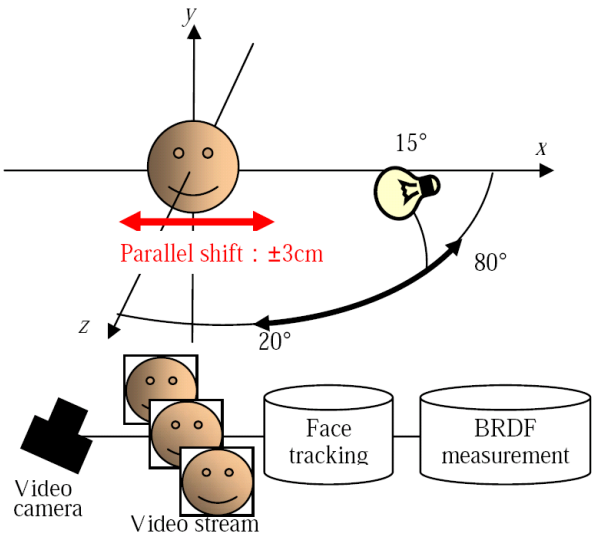

Figure 10: Geometry of BRDF measurement experiment.

truth of this experiment. Another one is the condition that the face is not kept still and its movement is not tracked. The last one is the condition that the face is not kept still and its movement is tracked by the proposed facial tracking. The face is moved randomly from side to side when the face is not kept still. The distance of the movement is up to 3cm. Figure 11 shows measured BRDFs. In the results of forehead, cheek and lip, BRDF with the face tracking is highly consistent with the ground truth. However, in the result of nose, BRDF with the face tracking is very different from the ground truth. It is thought that this difference is caused by the shading on the nose.

Application: moles and acnes removal simulation

As the application of our video-based analysis system, we performed moles and acnes removal simulation. The removal simulation can be performed by controlling skin color of moles and acnes. Positions of moles and acnes on the facial skin are tracked by the proposed tracking method. The skin color control[1] is performed to pixels in the small region around the target point. Figure 12(a) shows the removal simulation of moles, and (b) shows the removal simulation of acnes. Moles and acnes look like skin-like color parts.

Conclusion and Discussion

This paper proposed a video-based analysis for the appearance on the facial skin with an automatic face tracking technique. The facial movement can be tracked robustly against the shading by using the lip and the head center that are less influenced by the shading. The videobased analysis system could measure the BRDF of the moving face. In addition to the BRDF measurement, we performed moles and acnes removal simulation as the application of our video-based analysis system.

For further study, we must improve the tracking technique to track parallel shift along the z axis and roll rotation. It is thought that every movements of the face can be tracked accurately by using accurate 3D face model. Therefore, we are planning to reconstruct 3D face model and use to track.

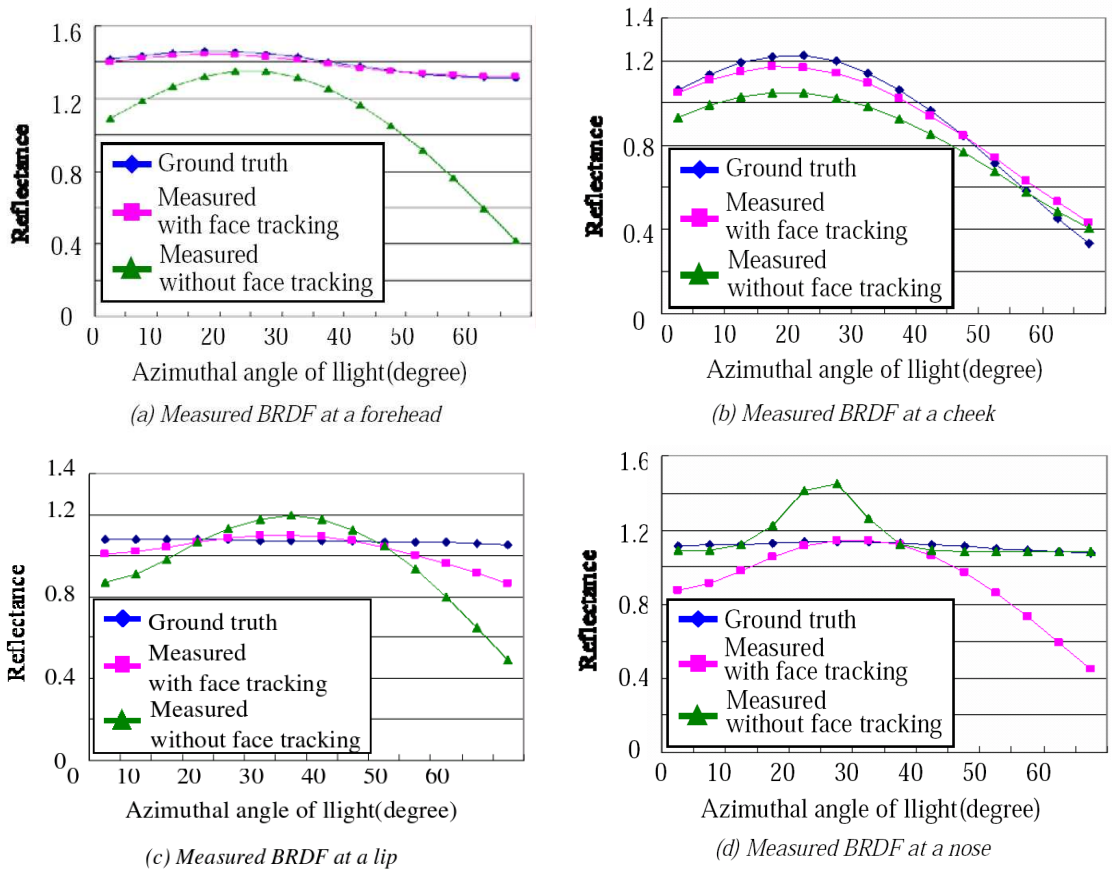

Figure 11: Results of BRDF measurement, (a)forehead, (b)cheek, (c)lip, (d)nose BRDFs.

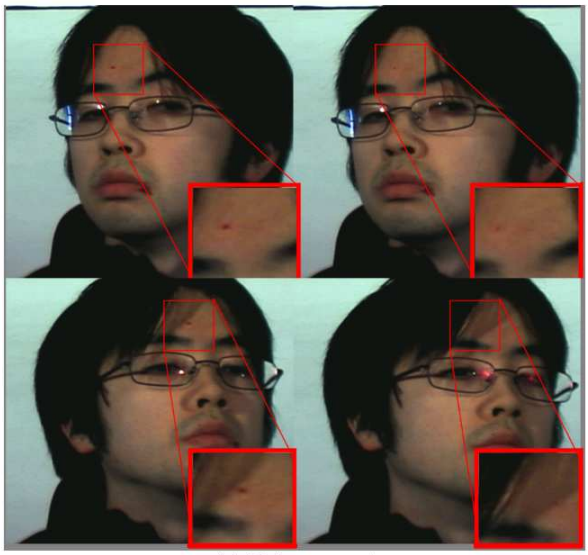

(a) Moles removal

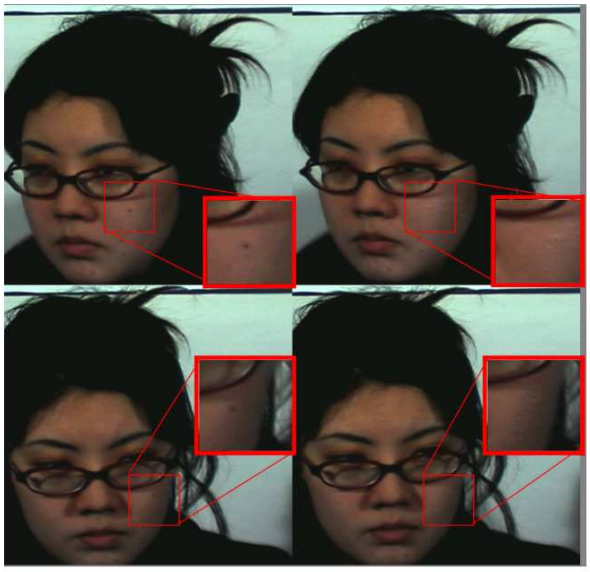

(b) Acnes removal

Figure 12: Removal simulation of moles and acnes.

References

[1] N. Tsumura, T. Nakaguchi, N. Ojima, K. Takase, S. Okaguchi, R. Usuba, M. Shiraishi, N. Okiyama, K. Hori and Y. Miyake: "Real-time image-based control of skin melanin texture", ACM SIGGRAPH2005 sketches (2005.8.3, LA, USA)

[2] I. Craw, H. Ellis, and J. Lishman: "Automatic Extraction of Face Features", Pattern Recognition Letters, vol. 5, pp. 183-187, 1987.

[3] S. Birchfield: "Elliptic al head tracking using intensity gradients and colour histograms", Proc. IEEE ICCVPR, pp232-237, 1998.

[4] Ward G. J: "Measuring and modeling anisotropic reflection", Computer Graphics Proceedings(ACM SIGGRAPH92) Vol.26 No.2 pp. 265-272. 1992.

[5] Y. Kuroda, K. Morioka, J. Lee, H. Yashima, H. Hashimoto: "Modified Hybrid Tracking Algorithm Using Mean Shift and Kalman Filter", In 2004 RISP International Workshop on Nonlinear Circuit and Signal Processing (NCSP'04), pp.177-180, 2004.03, Hawaii, USA.

New decomposition basis for reflectance recovery from multispectral imaging systems

Alamin Mansouri, Tadeusz Sliwa
Le2i, UMR-CNRS 5158, University of Burgundy, France

Jon Yngve Hardeberg
Gjøvik University College, Gjøvik, Norway

Yvon Voisin
Le2i, UMR-CNRS 5158, University of Burgundy, France

Abstract

In this paper, we deal with the problem of spectral reflectance functions estimation in the context of multispectral imaging systems. We work out in the linear model and we propose a novel method based on the use of spline wavelets as basis functions. We compare this method to Fourier and PCA basis. The results are evaluated with the commonly used goodness-of-fit coefficient (GFC) and prove the reliability of the use of wavelets.

Introduction

Conventional color imaging defines each pixel with 3 variables such as red, green and blue, which are necessary and sufficient to characterize any color. This principle has several limitations. First, in a color image acquisition process, the scene is acquired using a given illuminant. Thus, it is impossible to estimate the scene color accurately under another illuminant. Moreover, two color samples can match under one illuminant and appear completely different under another one. This phenomenon is called metamerism. Multispectral imaging systems remedy these problems by increasing the number of acquisition channels. In doing so, multispectral imaging provides the advantage of high spectral resolution over classical color imaging systems and the advantage of high spatial resolution over spectrophotometers. Furthermore, with such systems, scene surface reflectance recovery from the camera output becomes easier but not trivial. Thus, finding appropriate mathematical methods to estimate the spectral reflectance from the camera output is a crucial task and of great importance.

Problem formulation

The generally used spectral model of the acquisition chain in a multispectral system is illustrated in Figure 1, where $I(\lambda)$ is the spectral radiance of the illuminant, $r(\lambda)$ is the spectral reflectance of the surface, $o(\lambda)$ is the spectral transmittance of the optical system, $t_k(\lambda)$ is the spectral transmittance related to the kth filter, $c(\lambda)$ is the spectral sensitivity of the camera, and η_k represents the spectral noise for the k-th channel, $k = 1 \dots K$.

The camera output d_k, related to the channel k for a single pixel of the image, is given by

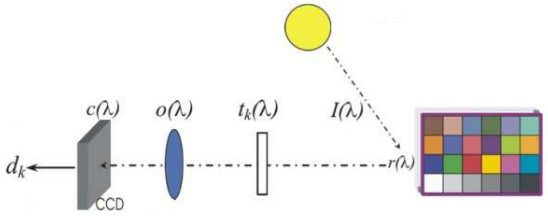

Figure 1: Synopsis of the spectral model of the acquisition process in a multispectral system.

$$d_k = \int_{\lambda_{min}}^{\lambda_{max}} I(\lambda) r(\lambda) o(\lambda) c(\lambda) t_k(\lambda)\, d\lambda + \eta_k. \tag{1}$$

If the noise is assumed removed by preprocessing [1], and assuming a linear opto-electronic transfer function, we can replace $I(\lambda)$, $c(\lambda)$, $o(\lambda)$ and $t_k(\lambda)$ by the spectral sensitivity $S_k(\lambda)$ of the kth channel. Then, the Equation (1) becomes:

$$d_k = \int_{\lambda_{min}}^{\lambda_{max}} S_k(\lambda) r(\lambda)\, d\lambda + \eta_k. \tag{2}$$

By regularly sampling the spectral range to N wavelengths, Equation (2) can be written in matrix notations as follows:

$$d_k = S_k^T(\lambda) r(\lambda), \tag{3}$$

where $S_k(\lambda) = [s_k(\lambda_1) s_k(\lambda_2) \dots s_k(\lambda_N)]^T$ is the vector containing the spectral sensitivity of the acquisition system related to the k-th channel, $r(\lambda) = [r(\lambda_1) r(\lambda_2) \dots r(\lambda_N)]^T$ is the vector of the sampled spectral reflectances of the scene, and T is the transpose operator. Considering the system with all channels, Equation (3 can be written as:

$$d = S^T r \tag{4}$$

where d is the vector containing all d_k camera outputs and $S = [s_1 s_2 \dots s_K]^T$ is the matrix containing the channels spectral sensitivities S_k. The final goal is to recover $r(\lambda)$ from the camera output according to Equation (4). This is obtained by finding an operator Q that solves for the following equation:

$$r = Qd. \tag{5}$$

Depending on how the operator S is determined, two paradigms of spectral reflectance estimation exist [2].

- If S is obtained by a direct physical system characterization, Q is the pseudo-inverse of S.
- If S is obtained indirectly by matching a set of M color patches (for which we know the theoretical reflectances) and we capture an image of these patches with the multispectral camera, we have then a set of corresponding pairs (d_m, r_m), for $m = 1, \dots, M$, where d_m is a vector of dimension K containing the camera responses and r_m is a vector of dimension N representing the spectral reflectance of the m-th patch. The reflectances r_m are gathered in the matrix R and the camera outputs for the M patches are gathered in the matrix D. The operator Q is straightforwardly obtained by calculation of this matching. Any optimization method can fulfill this aim (neural networks, Least squares...). Thus, the operator Q is obtained like:

  $$R = QD \tag{6}$$

  involving then the inversion

  $$Q = RD^{-1}. \tag{7}$$

A third paradigm for spectral reflectance estimation consists of direct interpolation of the camera outputs d_k. Then, no knowledge about operator S is required. Nevertheless, rigorous conditions about filters' shape, as well as well calibrated and normalized data is required for this kind of reconstruction. The reconstruction is performed by any interpolation operator (spline, etc.)

The final goal is to estimate spectral reflectance functions r from camera outputs d. To do so, several methods belonging to the two first paradigms exist in literature. Some classical approaches use the pseudo-inverse calculus and the least squares. The main drawback of these methods is instability of solutions due to the noise amplification. That is why some other methods add some constraints on the reflectance functions to be in the range [01] or seek to maximize the smoothness of the estimated result.

Reflectance estimation in the linear model

Utilization of a linear model to estimate reflectance from camera response seems to be trivial since we supposed a linear opto-electronic transfer function enabling us the matrix notation in Equations (4, 5). Moreover, the linear model offers an alternative to imposing smoothness on reflectance functions [3]. This is expressed by assuming that $r(\lambda)$ can be approximated by a linear combination of a small number of basis functions [4]. Thus, a set of basis functions B_j $(j = 1 \dots M))$ are defined such that each reflectance r_i could be written as:

$$r_i = B_j a_{i,j}, \tag{8}$$

where $a_{i,j}$ is the weight of the jth basis function related to the ith sample. The basis functions are themselves functions of wavelength but free of constraints such as being positive or constrained to be limited to the range [01]. Their number M is chosen to conserve maximum of energy. Equation (4) can be written as:

$$d = S^T B a, \tag{9}$$

where the columns of the $N \times M$ matrix B contain the M basis functions of a linear model of reflectance spectra and the $M \times 1$ matrix a holds the weights that define the particular spectrum that we are trying to reconstruct. When gathering S^T and B in a unique operator, the latter is a square matrix that could be easily inverted. We can rewrite Equation (9 as:

$$a = (S^T B)^{-1} d, \tag{10}$$

which allows us to compute a. Afterwards we can easily estimate r by simple multiplication:

$$r = Ba. \tag{11}$$

In this context, methods belonging to the second paradigm use techniques of decomposition, although implicitly. We can cite the method proposed [5] which takes advantage of the a priori knowledge about the spectral reflectances that are to be imaged (pigments reflectance for paintings reflectance reconstruction). Methods based on linear neural networks are also methods taking benefits from basis decomposition [6]. In our paper we will achieve the decomposition task by experimenting with three basis functions: PCA, Fourier and Wavelets analysis.

Experiments and results

In this section, we describe three experiments to evaluate the spectral reflectance estimation performance for the three methods: PCA, Fourier and wavelets analysis. The data we used are sampled at 10 nm intervals in the range $[400, 700]$ yielding for each spectrum $r(\lambda)$ to a vector of 31 values.

The aim of this experiment is to derive a small number of basis functions from a set of spectra using the three methods. Then, we try to reconstruct all the set using only the basis we computed. To do this we used a set of 404 natural spectra. We performed decomposition using the three methods. We found that 95% of energy is hold by the six greatest vectors. Furthermore, for practical reasons that involve the number of Fourier and wavelets basis to be multiple of two, we chose to keep the eight first basis functions. The wavelets we used in this paper are based on the spline family.

Reconstruction of training set

After deriving the basis functions for the "training" set, we try to reconstruct all the spectra in this set using these basis functions and the coefficients matrix a (Equation (10). The Figure 2 shows the results for the three methods in terms of visual comparison of reconstructed curves:

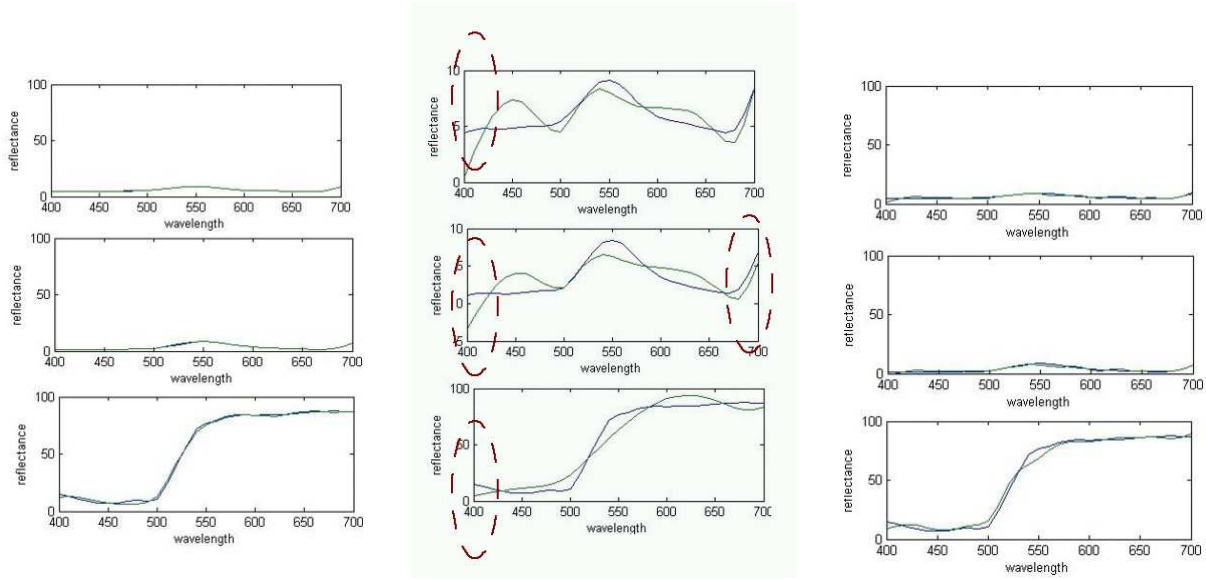

Figure 2: Samples of reconstructed spectra from the training set using: a. PCA eight basis functions, b. Fourier eight basis functions, c. Wavelets eight basis functions.

Table 1: Results, in terms of GFC, of the reconstruction of the training set for the three methods.

Method	GFC			
	Mean	median	STD	Min
PCA	0.9997	0.9999	$5.1903 \cdot 10^4$	0.9953
Fourier	0.9841	0.9905	0.0170	0.8799
Wavelets	0.9952	0.9978	0.0053	0.9655

We also evaluate the reflectance estimation in terms of an objective metric. For this purpose, we used the non centered correlation coefficient, largely used and known in the community as Goodness of Fit Coefficient (GFC) expressed by the formula:

$$GFC = \frac{\left|\sum_j R_m(\lambda_j) R_r(\lambda_j)\right|}{\left(\left|\sum_j R_m(\lambda_j)^2\right|\right)^{1/2} \left(\left|\sum_j R_r(\lambda_j)^2\right|\right)^{1/2}}$$

where $R_m(\lambda_j)$ is the value measured by the spectrophotometer in the wavelength λ_j, and $R_r(\lambda_j)$ represents the reconstructed value related to the same wavelength. Table 1 gives the full results for the 404 spectra in terms of mean, median, standard deviation and the minimal value of GFC.

Generalization performance

From the previous results, we retain PCA and Wavelets to test them in the task of generalization. That means we extract a PCA and wavelets basis functions from a set that we call training set and try to estimate reflectance from another set. In our case, we used Macbeth DC as a training set and Macbeth Color checker as reconstruction target. Figure 3 depicts some samples of the performed reconstruction allowing for visual comparison of the reconstructed curves. We also evaluate the generalization capabilities of these two methods in terms of GFC. Table 2 gives the results.

Table 2: Results, in terms of GFC, of the generalization capabilities for the methods using PCA and wavelets basis functions

Method	GFC			
	Mean	median	STD	Min
PCA	0.9971	0.9990	0.0048	0.9820
Wavelets	0.9980	0.9986	0.0021	0.9922

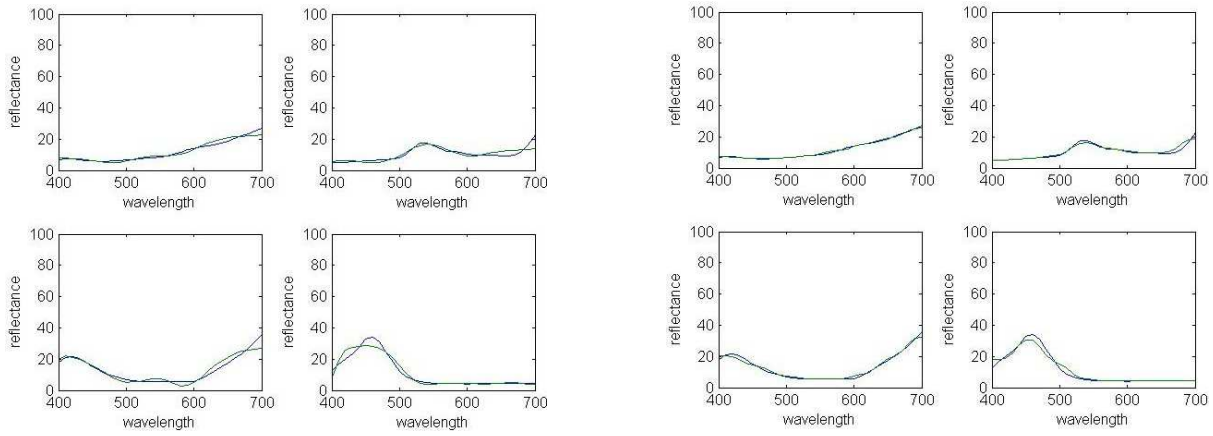

Figure 3: Results of generalization test for: a. PCA basis functions and b. Wavelets basis function.

Estimation from multispectral image

The main objective in multispectral imaging is to be able to reconstruct full spectral reflectance curves $r(\lambda)$ from a small number of channels K contained in the vector d_k. That is why we perform this third experiment. We used two multispectral images of the Macbeth DC composed of eight channels representing captured each 40 nm in the range $[400, 700]$. The difference between the two images is the shape of the filters. The first image is issued from narrow-band filters, while the second image is issued from large-band filters (FWHM of 40 nm). Then, in order to recover the full spectrum for each patch, we used the previously computed basis in the case of the wavelets but we computed a new basis for the PCA method. Figure 4 shows results for this experiment in terms of visual comparison of curves.

Table 3 gives the results for this experiment in terms of GFC when using a multispectral image issued from narrow band filters.

The Table 4 gives the results for this experiment in terms of GFC when using a multispectral image issued from large band filters.

Table 3: Results, in terms of GFC, for the reflectance estimation from camera outputs in the case of multispectral image from narrow-band filters.

Method	GFC			
	Mean	median	STD	Min
PCA	0.8841	0.9605	0.1898	0.2847
Wavelets	0.9948	0.9972	0.0064	0.9710

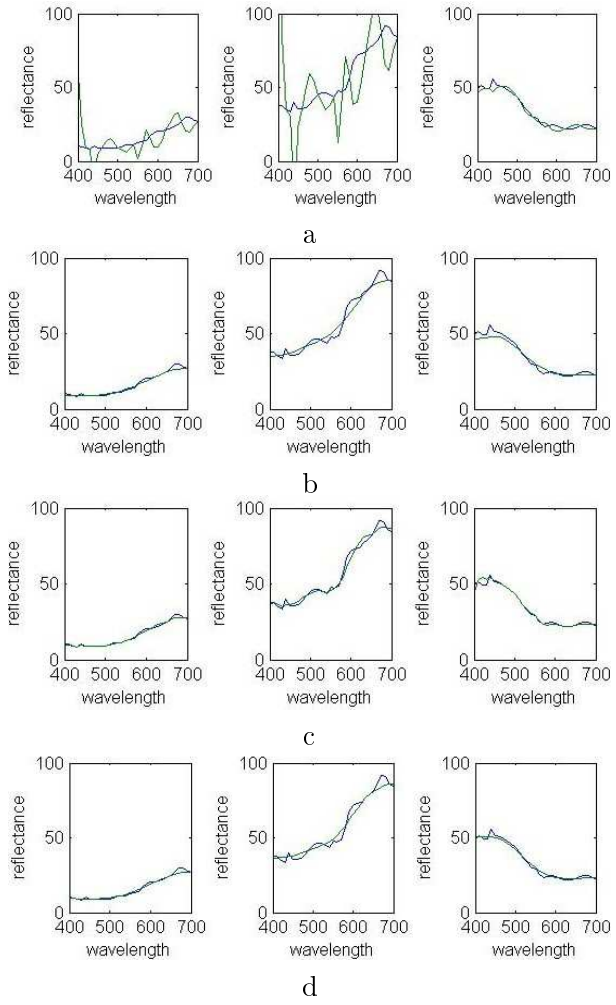

Figure 4: Results of reflectance estimation from: a. narrow-band multispectral image using PCA, b. narrow-band multispectral image using wavelets, c. large-band multispectral image using PCA, and d. large-band multispectral image using wavelets

Table 4: Results for the reflectance estimation from camera outputs in the case of multispectral image from large-band filters.

Method	GFC			
	Mean	median	STD	Min
PCA	0.9970	0.9993	0.0081	0.9604
Wavelets	0.9948	0.9971	0.0071	0.9665

Discussion

Looking to the results of the first experiment, one can remark that Fourier basis presents the worst performances and presents some artifacts on the boundaries as depicted in Figure 2b (encircled area); this even we replicate periodically the reflectance samples. The wavelets remedy to this problem thanks to multiresolution analysis and presents therefore good results in terms of GFC and visual comparison. But, the PCA presents the greatest scores for the task of reconstructing samples from the training set. It is natural since PCA derive Smooth basis for smooth data set. For the generalization task, the wavelets basis functions performs better and get the best scores in term of GFC and curves visual comparison even the training set and test set are statistically similar (Macbeth DC and Macbeth CC). We notice that we could use the basis functions derived from the first experiments in the case of wavelets. Wavelets basis are independent from training. The only hypothesis is that the curves are smooth. The third experiment shows again the best performance of the wavelets in the task of estimating reflectances from multispectral output system. In the case of multispectral image issued from narrow-band filters, scores for the wavelets are largely superior. That means that PCA is not adapted to reconstruction for this kind of images. In the case of multispectral image issued from large-band filters, the two methods presents quite similar results. The mean and median are superior for PCA but the standard deviation and the min are superior for Wavelets. That expresses the stability in the results of wavelets.

Conclusion

In this paper, we introduced a new method for spectral reflectance reconstruction using wavelets basis functions. We tested this method in three cases: reconstruction of the training set, generalization and the reconstruction of reflectance from multispectral imaging system. We compare this method to two other methods belonging to the same paradigm: Fourier and PCA. We evaluate the results in terms of GFC and reflectance curves comparison. The proposed method show good and stable performance in all experiments. The future work will concern designing and testing other types of wavelength more adapted to smooth reflectances.

References

[1] Mansouri, F. S. Marzani, P. Gouton, Development of a protocol for CCD calibration: application to a multispectral imaging system, Intl. Journal of Robotics and Automation, Acta Press, 20 (2), 94-100 (2005).

[2] A. Ribes-Cortes, Analyse multispectrale et reconstruction de la reflectance spectrale de tableaux de maître, PhD thesis, ENST Paris, december (2003).

[3] D. Connah, , J. Y. Hardeberg and S. Westland, Comparison of linear spectral reconstruction methods for multispectral imaging, IEEE-International Conference on Image Processing (ICIP04), 1497-1500 (2004).

[4] L. T. Maloney, Evaluation of linear models of surface spectral reflectance with a small number of parameters, Journal of the Optical Society of America - A, 3 (10), 1673.1683 (1986).

[5] J. Y. Hardeberg, F. Schmitt and H. Brettel, Multispectral color image capture using liquid crystal tunable filter, Optical Engineering, 41(10), 2532-2548 (2002).

[6] Mansouri, F. S. Marzani and P. Gouton, Neural networks in cascade schemes for spectral reflectance reconstruction , IEEE-International Conference on Image Processing (ICIP05), II, 718-721 (2005).

Spectral Color Reproduction versus Color Reproduction

Jérémie Gerhardt and Jon Y. Hardeberg
The Norwegian Color Research Laboratory
Department of Computer Science and Media Technology
Gjøvik University College, Gjøvik, Norway

Abstract

In this paper we are comparing spectral color reproduction versus color reproduction. We perform three colorant separations based on the inversion of the spectral Neugebauer model: one minimizing a spectral difference for the spectral print, a second minimizing a colorimetric difference for the colorimetric print and a third one minimizing a weighted summation of both colorimetric and spectral difference. A multi-colorant printer is used for our experiments and the prints simulated with the spectral Neugebauer model.

Keywords: spectral color reproduction, spectral printer model, multi-colorant printing, spectral colorant separation.

1. Introduction

With a color reproduction system it is possible to make a color acquisition of a scene or object under a given illuminant and to print a color reproduction of it. With proper calibration and characterization of the devices involved, and disregarding the problems related to color gamut limitations, it is theoretically possible to produce a color reproduction which will appear identically to the original. For example a painting and its color reproduction put side by side will appear identical under the illuminant used for its color acquisition even if the spectral properties of the painting pigments are different from the print inks. This phenomenon is called metamerism. On the other hand, if the illumination changes, the reproduction will generally no longer be perceived as equal to the original. This problem can be solved in a spectral color reproduction system.

Multispectral color imaging offers the great advantage to provide the full spectral color information of a surface. While a color acquisition system records the color of a surface under a given illuminant, a multispectral acquisition system can record the spectral reflectance of a surface and allows us to simulate the color of under any illuminant. In an ideal case, after saving a spectral image we would like to display or to print it, from that point we have two options: either to calculate the color rendering of our spectral image for a given illuminant and to display/print it, or to reproduce the spectral image. This is a challenging task when for example we have made the spectral acquisition of a 2 century old painting and the colorants used at that time are not available anymore or we have lost the technical knowledge to produce them.

The introduction of multi-colorant printer in color printing, for a primary goal of increasing printer color gamut has offered new possibilities in spectral color reproduction. The first works with a spectral use of multi-colorant printer were focused on colorant selection [1, 2, 3] and spectral printer modeling [4, 5]. Then spectral color reproduction of spectral image was introduced [6, 7, 8]. A complete workflow for spectral color reproduction is existing and research works are converging toward linking acquisition and reproduction of spectral image [9, 10] based on the model of a color reproduction workflow.

Multi-colorant printer offers the possibility to print the same color by various colorant combinations, i.e. metameric print is possible. This is an advantage for colorant separation [11, 12], it allows for example to select colorant combination minimizing colorant coverage or to optimize the separation for a given illuminant. In spectral colorant separation we are aiming to reduce the spectral difference between a spectral target and its reproduction, i.e. we want to reduce the metamerism. This task is performed by inverting the spectral printer model.

The spectral Neugebauer model and the Yules-Nilsen spectral modified Neugebauer model (YNSN) are commonly use for spectral printer characterization [13]. As in color reproduction such system needs to be characterized and spectral printer characterization has been used already for color reproduction since it provided more accurate information [5].

2. Spectral versus colorimetric printing

In this paper we want to asses the difference between a multi-spectral print and a colorimetric print. The choice of colorimetric versus spectral printing is made during the colorant separation process. Colorant separation (i.e. inversion of the spectral printer model) is performed by optimization technique ending by minimizing a cost function. When a spectral print is desired the colorant separation is performed such that the difference between the spectral target and the estimated print is minimized for the spectral root mean square (sRMS) difference. For a colorimetric print we will calculate a ΔE^*_{ab} difference between the spectral target and the estimated print.

Gamut mapping plays an important role in color reproduction: printer gamut and image gamut may be partially different. Gamut mapping transformation will map image data to the printer gamut in order to keep most of the information [14]. Gamut mapping becomes more complicated for spectral data [15], due to the dimension of the problem it is likely impossible to apply directly color gamut mapping techniques to spectral data. But with the use of an inverse printer model and optimization it is possible to map spectral reflectance to the spectral printer gamut. The spectral printer gamut is defined by the spectral reflectance of the available colorants and all the combination between them, i.e. the Neugebauer primaries (NP) of the printer. According to the Neugebauer printer model the spectral reflectance of a printed colorant combination is the weighted summation of the NP where the weights are the area covered by the NP. It is a convex optimization problem to solve since the summation of the weights is equal to 1. So by inverting the spectral Neugebauer model for the weights we obtain an estimation of the closest printable spectral reflectance according to the desired spectral target and colorants [16].

3. Experiment and results

We use in our experiment the Esser testchart made of 283 spectral patches. Colorimetric and spectral prints are simulated for the original testchart and its gamut mapped version with the technique described above, see in Fig. 1 (a) the gamut mapped Esser testchart spectral reflectances. The colorant separations are run for a simulated seven colorants printer, see Fig. 1 (b) for the NP spectral reflectances of the printer.

Performance of the colorant separation processes are shown in Table 1 for the original testchart and Table 2 for the gamut mapped testchart. In both experiment the colorimetric print is performed for ΔE^*_{ab} under illuminant D50. Differences between target and print are calculated in CIE$L^*a^*b^*$ space for illuminant A, D50, D65, F11 and sRMS.

A third method is experimented to perform the colorant separation involving both sRMS and ΔE^*_{ab} in the cost function. Our metric is then a weighted summation of these two metrics and the difference to be minimized is defined by:

$$d = (1 - \alpha) \times \Delta E^*_{ab} + \alpha \times \text{sRMS} \tag{1}$$

where $\alpha = 0$ is equivalent to colorimetric print and $\alpha = 1$ equivalent to spectral print. sRMS has been scaled for this method such that both metric vary in the same range of value. In Fig. 2 (a) are displayed colorimetric differences and in Fig. 2 (b) spectral differences versus α. Extreme values in the graphs are corresponding to those displayed in Tab. 2.

We observe an interesting result, from $\alpha = 0$ to $\alpha = 0.25$ the sRMS metric is decreasing faster than the increasement of the colorimetric metric ΔE^*_{ab}. Small α values corresponds to

bigger weigth put on the colorimetric difference in the colorant separation. This method seems to reach an area where the ΔE^*_{ab} is stable and sRMS is decreasing. It describes colorant values which both minimizes colorimetric and spectral difference.

4. Conclusion

Both method end up with large error when colorant separation is performed on the original data. But the spectral print produce smaller error in term of spectral difference than for the colorimetric print and colorimetric print produce smaller colorimetric difference with a minimum peak for the illuminant D50 chosen during the colorant separation, see Tab. 1 and Tab. 2.

After spectral gamut mapping both method provide closer prints with the new gamut mapped testchart. We can see that the spectral print is still better than the colorimetric print in term of spectral difference. But all colorimetric differences are reduced for the colorimetric print and are minimum again for the illuminant used in the colorant separation. The colorant separation including a minimization of a metric based on both colorimetric and spectral confirms that more weight put on the colorimetric difference or on the spectral difference improves one or the other difference respectively and still a better spectral difference does not provide better colorimetric differences. But it also reveals an area corresponding to small α value where both colorimetric and spectral metrics are decreased.

A spectral print tends to reduce metamerism (smaller variations between the colorimetric differences comparing to those obtain for colorimetric print) but other targets and set of colorant should be tested for the colorant separation process. Also the use of the inverse YNSN should provide better results since it improves the spectral Neugebauer model.

References

[1] Timothy Kohler and Roy S. Berns. Reducing metamerism and increasing gamut using five or more colored inks. *IS&T's Third Technical Symposium On Prepress, Proofing, and Printing*, pages 24–29, 1993.

[2] Di-Yuan Tzeng and Roy S. Berns. Spectral based ink selection for multiple-ink printing II. optimal ink selection. *The Seventh Color Imaging Conference: Color Science, Systems, and Applications*, pages 182–187, November 1999.

[3] Di-Yuan Tzeng and Roy S. Berns. Spectral-based six-color separation minimizing metamerism. In *IS&T/SID Eight Color Imaging COnference*, pages 342–347, November 2000.

[4] David R. Wyble and Roy S. Berns. A critical review of spectral models applied to binary color printing. *Color Research Application*, 25(1):4–19, 2000.

[5] Raja Balasubramanian. Optimization of the spectral neugebauer model for printer characterization. *Journal of Electronic Imaging*, 8(2):156–166, April 1999.

[6] Lawrence A. Taplin and Roy S. Berns. Spectral color reproduction based on a six-color inkjet output system. *The Ninth Color Imaging Conference*, pages 209–212, November 2001.

[7] Roy S. Berns, Lawrence A. Taplin, and Tony Z. Liang. Spectral color reproduction with six color output. US patent 0098896A1, May 2003.

[8] Andreas Kraushaar and Philipp Urban. How to linearise a multispectral printing system for graphic arts uses? In *IARIGAI Proceedings 33rd International Research Conference*, 2006.

Table 1: Differences between the colorimetric and spectral print for the original Esser testchart.

method		ΔE^*_{ab} A	D65	D50	F11	sRMS
spectral	Av.	13.32	15.57	14.99	15.73	0.047
	Std	11.92	13.34	12.74	12.44	0.035
	Max	65.37	70.16	68.86	69.90	0.180
D50	Av.	9.43	9.03	8.72	10.09	0.073
	Std	9.89	9.75	9.96	9.35	0.048
	Max	52.39	45.85	44.45	42.39	0.255

Table 2: Differences between the colorimetric and spectral print for the gamut mapped Esser testchart. The first three line show the differences between the original testchart and the gamut mapped testchart.

method		ΔE^*_{ab} A	D65	D50	F11	sRMS
spectral	Av.	12.01	13.87	13.40	14.13	0.044
gamut	Std	11.33	12.36	11.87	11.86	0.035
mapping	Max	59.98	63.98	60.33	61.23	0.180
	Av.	1.66	1.83	1.78	1.90	0.005
spectral	Std	2.73	2.62	2.65	2.95	0.005
	Max	14.38	13.40	13.77	16.42	0.026
	Av.	1.48	1.12	0.99	1.40	0.013
D50	Std	2.36	1.91	2.12	2.30	0.012
	Max	14.84	11.87	12.81	13.01	0.089

[9] Mitchell R. Rosen, Edward F. Hattenberger, and Nobotu Ohta. Spectral redundancy in a 6-ink ink-jet printer. *IS&T 2003 PICS Conference*, pages 236–243, 2003.

[10] Maxim W. Derhak and Mitchell R. Rosen. Spectral colorimetry using LabPQR: an interim connection space. *Journal of Imaging Science and Technology*, 50(1):53–63, 2006.

[11] Victor Ostromoukhov. Chromaticity gamut enhancement by heptatone multi-color printing. In *IS&T SPIE*, volume 1990, pages 139–151, 1993.

[12] A. Ufuk Agar. Model based color separation for cmykcm printing. In *The 9th Color Imaging Conference: Color Science and Engineering: Systems, Technologies, Applications*, 2001.

[13] Jon Y. Hardeberg and Jérémie Gerhardt. Characterization of an eight colorant inkjet system for spectral color reproduction. pages 263–267, 2004.

[14] Ján Morovič and M. Ronnier Luo. The fundamentals of gamut mapping: A survey. *Journal of Imaging Science and Technology*, 45(3):283–290, 2001.

[15] Arne M. Bakke, Ivar Farup, and Jon Y. Hardeberg. Multispectral gamut mapping and visualization – a first attempt. In *Color Imaging: Processing, Hardcopy, and Applications X, Electronic Imaging Symposium*, volume 5667 of *SPIE Proceedings*, pages 193–200, San Jose, California, January 2005.

[16] Ali Alsam, Jérémie Gerhardt, and Jon Y. Hardeberg. Inversion of the Spectral Neugebauer Printer Model. In *AIC Colour 05*, pages 44–62, 2005.

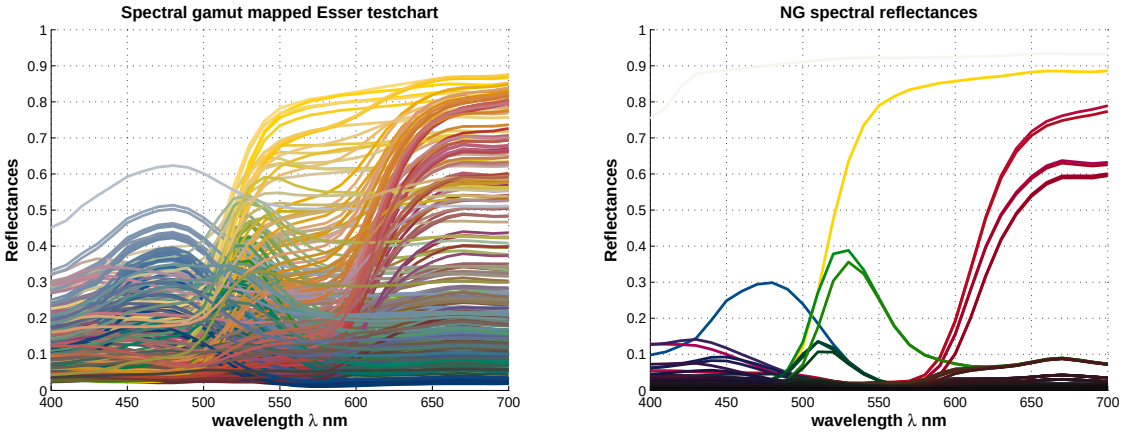

(a) (b)

Figure 1: Spectral reflectance of the Esser teschart after spectral gamut mapping in (a). The 128 Neugebauer primaries spectral reflectances used for gamut mapping and simulating the spectral and colorimetric prints in (b).

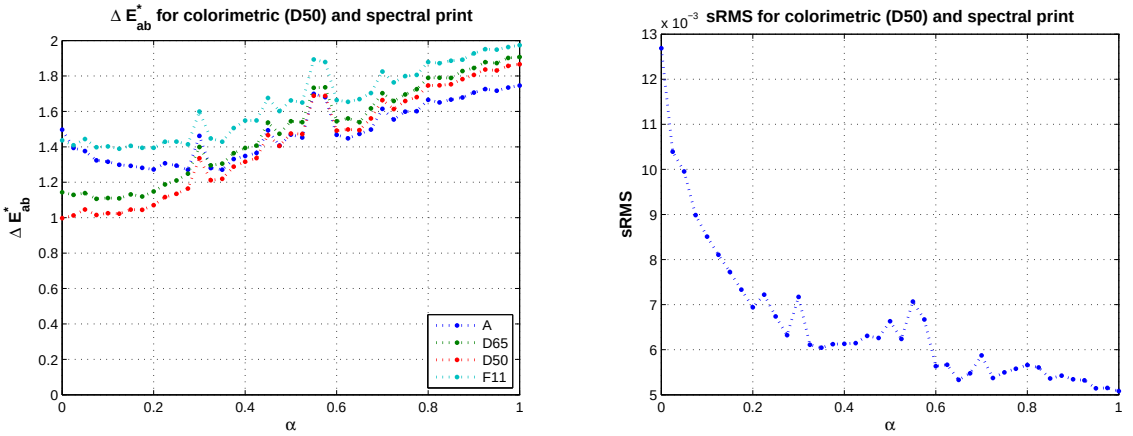

(a) (b)

Figure 2: Evolution of the difference between the original target (here the gamut mapped Esser testchart) and the its estimation after colorant separation function of α factor. ΔE^*_{ab} in (a) and sRMS in (b).